ROCK CLASSIFICATION IN ORGANIC SHALE BASED ON PETROPHYSICAL AND ELASTIC ROCK PROPERTIES CALCULATED FROM WELL LOGS

A Thesis

by

ALVARO A. ARANIBAR FERNANDEZ

Submitted to the Office of Graduate and Professional Studies of
Texas A&M University
in partial fulfillment of the requirements for the degree of

MASTER OF SCIENCE

Chair of Committee,	Zoya Heidari
Committee Members,	Walter B. Ayers
	Michael Pope
Head of Department,	A. Daniel Hill

December 2014

Major Subject: Petroleum Engineering

ABSTRACT

This thesis introduces a rock classification technique for organic-rich shale that takes into account well-log-based estimates of compositional, petrophysical, and elastic properties.

Well logs and laboratory core measurements were used to calculate depth-by-depth petrophysical and compositional properties of three wells in two organic-rich formations. Then, either acoustic well logs or effective medium theories helped estimate formation elastic properties. Estimates of total porosity, Total Organic Content (TOC), fluid saturation, volumetric concentrations of mineral constituents, and elastic properties facilitated identification of different rock classes, using an unsupervised artificial neural network. A good rock classification technique improves (a) petrophysical evaluation of organic-rich shale reservoirs, (b) fluid flow characterization, (c) detection of productive zones for fracturing jobs, and (d) prediction of hydraulic fracturing and stimulation effectiveness.

Then, a rock classification method was then applied to the field examples from the Haynesville shale and Woodford shales for rock classification. The estimates of porosity, TOC, bulk modulus, shear modulus, and volumetric concentrations of minerals were obtained and then validated by comparing them to laboratory measurements. These calculated properties and well logs served as inputs to an artificial neural network to identify the different rock classes in both formations. Finally, the rock classes enabled identification of good candidate zones for fracture stimulation.

DEDICATION

To my mom, dad, brother, and sister for their support and unconditional love.

ACKNOWLEDGEMENTS

This thesis would not have been possible without the support, encouragement, and patience of my advisor and committee chair, Dr. Zoya Heidari. I also thank the members of my committee, Dr. Walter B. Ayers and Dr. Michael C. Pope for their time and effort reviewing my thesis.

The work and research reported in this thesis was funded by the Multi-Scale Formation Evaluation Research Group, jointly sponsored by Aramco Services Company, BHP Billiton, BP, Chevron, ConocoPhillips, and Devon Energy. I also thank Schlumberger for allowing the use of the well-log interpretation software TechLog (Mark of Schlumberger) free of charge. I thank the Harold Vance Department of Petroleum Engineering staff for being extremely helpful during my time in the department.

I also sincerely thank my friends and colleagues at Texas A&M University. Special thanks go to Nikhil Kethireddy, Clotilde Chen, and Mehrnoosh Saneifar for their help and support of my research. I also thank all my office mates for maintaining an awesome and promoting work environment. A big thank you goes to Gia Alexander for her help on editing this thesis. Finally, I thank my parents, my brother, and my sister for their continuous support.

NOMENCLATURE

List of Acronyms

DEM	Differential Effective Medium
ECS	Elemental Capture Spectroscopy
GR	Gamma Ray
LOM	Level of Organic Metamorphism
PEF	Photoelectric Factor
SCA	Self-Consistent Approximation
SEM	Scanning Electron Microscope
TOC	Total Organic Content
XRD	X-Ray Diffraction

List of Symbols

E	Young's Modulus
K	Bulk Modulus
K_{dry}	Dry Bulk Modulus
K_{sat}	Saturated Bulk Modulus
K_f	Pore Filling Fluid Bulk Modulus
K^*	Effective Bulk Modulus

N	Total Number of Rock Inclusions
P^*_i	Mineral Inclusion Shape Factor
Q^*_i	Mineral Inclusion Shape Factor
R	Deep Resistivity Log
S_d	Deviatoric Stress
Vp	Compressional-wave Velocity
Vs	Shear-wave Velocity
X	Volumetric Fraction of Rock Components
ρ	Bulk Density
ε_v	Volumetric Strain
ε_a	Axial Strain
ϕ	Total Porosity
σ'_c	Confining Hydrostatic Pressure
μ	Shear Modulus
μ^*	Effective Shear Modulus
υ	Poisson's Ratio

TABLE OF CONTENTS

Page

LIST OF FIGURES

LIST OF TABLES

1. INTRODUCTION

Projected hydrocarbon recovery from organic-shale reservoirs has increased, from 2% to estimates of about 50%, over the past decade due to technological developments such as horizontal drilling and hydraulic fracturing (King 2010). The ability to unlock the hydrocarbon reserves in organic-shale reservoirs has transformed these formations into economical performers in the oil and gas industry. Hydrocarbon production from organic-rich shale, however, due to their complex nature, remains challenging. Permeabilities in the nano-Darcy range and low porosity make hydraulic fracturing essential to achieve the best connection between the reservoir and the wellbore in these formations. An optimal completion design, which includes zone selection based on petrophysical, compositional, and elastic properties, results in an efficient and economical response of the formation to fracture stimulation. Oil companies can reduce completion costs by minimizing the number of fractures necessary to complete a well successfully. Therefore, the challenge of identifying the best intervals to complete has made petrophysical and compositional evaluation in organic-rich shale critical for the petroleum industry.

Rock classification enhances fracture treatment design for successful field development in organic-rich formations. Mineral composition and elastic properties are important parameters to take into account when selecting the best candidate zones for fracture treatment. However, characterization of the rapid variation of petrophysical, compositional, and elastic properties in organic-rich shale remains challenging. Well logs

can be applied for the assessment of the properties of these formations at large depth intervals compared to core measurements.

1.1 Background

1.1.1 Multi-mineral analysis

Petrophysical evaluation of organic-rich shale remains a major technical challenge in the petroleum industry due to heterogeneous lithology, complex pore structure, and insufficient procedures for performing laboratory measurements in unconventional reservoir core samples (Ramirez et al. 2011).

Traditionally, empirical correlations have been the standard for compositional and petrophysical evaluation in organic-shale reservoirs; however, these techniques lack physical basis and are not always reliable for predicting the volumetric concentrations of minerals (Singh 2013). Furthermore, researchers validate well-log interpretation methods using laboratory core measurements. A study by Passey et al. (2010), describes the inconsistency of petrophysical properties measured by commercial laboratories. These uncertainties in the conventional calibration approach, in addition to the complexity of these reservoirs, carry over into in the well-log-based assessment of petrophysical properties, thus increasing the error in compositional and petrophysical estimates.

Advances in well-log inversion techniques enable a comprehensive formation evaluation in organic-shale reservoirs. New techniques use non-linear inversion methods for joint interpretation of well logs to estimate TOC, water saturation, total porosity, and

volumetric concentrations of minerals (Heidari et al. 2012). An important advantage of these techniques is that they minimize the calibration effort against core measurements by using the well-log measurements to calibrate the outcomes.

1.1.2 Assessment of elastic properties in organic-rich shale

Elastic rock properties (e.g., Young's Modulus and Poisson's Ratio) provide information about the brittleness of a formation and its reaction to fracture treatment. Poisson's Ratio and Young's Modulus reflect the possibility of fracture initiation and the ability of the rock to maintain a fracture, respectively (Rickman et al. 2008). Gupta et al. (2012) and King (2010) also discuss the influence of Young's Modulus and Poisson's Ratio on the ability of the rock to be fractured. Both authors are in agreement with Rickman et al. (2008) on the possible increased fracture potential of rocks with high Young's Modulus and low Poisson's Ratio. Accounting for the elastic properties in organic-rich shale improves the reliability of rock classification and, thus, the assessment of economic viability of production sites.

Researchers apply acoustic velocity measurements to estimate elastic properties of the rock. However, the application of these measurements might not be reliable in the case of complex organic-rich shale (Jiang and Spikes 2013). Furthermore, compressional- and shear-wave velocity logs are affected by borehole conditions, as well as by abnormally high pore pressures in geopressured organic-rich shale (e.g., the Haynesville shale). Elevated pore pressures cause a slow-down in the first compressional arrival that does not represent the true elastic properties of the formation (Parker et al. 2009).

Montaut et al. (2013) explain the advantages of using effective medium theories for the assessment of elastic properties in organic- rich formations. These techniques take into account volumetric concentrations and shapes of different rock inclusions (i.e., minerals and pores); taking the mineral shapes into account gives a more accurate representation of the rock. Avseth et al. (2010) indicated that inclusion models such as the self-consistent approximation (SCA) and the differential effective medium (DEM) accurately approximate the rock as an elastic solid containing dry or fluid-filled inclusion that represents the pore space. Work by Guo et al. (2013) and Jiang and Spikes (2011) support that the SCA appropriately approximates bulk and shear moduli in organic-rich shale by taking into account multiple mineralogical phases, as well as their shapes and spatial distributions. An opposing idea describes that the elastic properties obtained from the SCA model might not be reliable in complex formations (Hornby et al. 1994). However, the authors reported that the SCA model, when combined with the Differential Effective Medium (DEM) model, improves estimates of elastic properties in complex formations because it starts by creating an interconnected porous media; then, inclusion are added to construct a model that represents the formation accurately (Hornby et al. 1994). In this thesis I perform a comparison between five widely used models in industry to determine which one represents the formations studied in this thesis the best.

1.1.3 Rock classification

Conventional rock classification techniques (Leverett 1941; Pittman 1992; Amaefule et al. 1993) are mainly dependent on porosity-permeability correlations obtained from core measurements. These techniques are applicable in carbonate and sandstone formations with a broad range of porosity and permeability, however, they are not reliable in organic- rich formations due to the narrower range of porosity and permeability and the significant uncertainty in laboratory measurements of these two properties (Sondergeld et al. 2010; Passey et al. 2010).On the other hand well-log based rock classification techniques have been shown useful as they provided continuous vertical measurements of the formation properties. The distinct responses of the well logs can be used for rock classification, these were define as electro facies (Serra and Abbott 1980).

A different approach to perform rock classification using well logs includes application of statistical methods (Ye et al. 1998; Lee and Datta-Gupta 2002; Silva et al. 2002). These statistical methods, however, require the data to follow a multivariate-normal distribution to identify accurately distinct rock classes. Organic-rich shale because of their heterogeneity, normally do not follow a multivariate-normal distribution; therefore, the application of these models may not result in an accurate rock classification. A more suitable method for well-log-based rock classification combines self-organizing maps with discriminant analysis to give results with over 80% accuracy in carbonate reservoirs (Skalinski et al. 2005)

Researchers have developed newer techniques for rock classification in organic-shale reservoirs since 2010; however, most of these approaches are strongly dependent on costly and hard-to-obtain core measurements (Gupta et al. 2012; Kale et al. 2010; Hammes et al. 2011; Marino et al. 2013). Furthermore, due to the complexity of organic-rich shale, hundreds of core samples can be required to detect the heterogeneity and capture variant rock features in the formation (e.g. porosity, elastic properties, and fluid saturation). For example, Gupta et al. (2012), classified 300 core samples from six different wells in the Woodford shale using Total Organic Content (TOC), porosity, and concentration of clay and quartz to classify rock types. A similar method for rock classification used 800 core samples in the Barnett shale (Kale et al. 2010). Yet another cumbersome core database from over 300 wells in the Haynesville shale was required to determine its lithofacies (Hammes and Frébourg 2012).

Recently, well-log based techniques have been developed to perform rock classification in organic-shale reservoirs (Popielski et al. 2012; Gamero-Diaz et al. 2013; Potma et al. 2013). Well logs work well for rock classification in organic- rich formations because they provide physical measurements of the formation, with a high vertical sampling resolution, compared to core measurements. Furthermore, the application of well logs enables a timely rock classification. To reduce shoulder bed effect on well logs, statistical techniques, such as k-means cluster analysis and factor analysis on conventional well logs, combined with well-log inversion, contribute to rock classification (Popielski et al. 2012). Popielski et al. (2012) explored whether well logs prove effective to perform rock classification in organic-shale reservoirs, and whether the inversion would improve

the results by minimizing the shoulder bed effect. The authors classified rock types in the Barnett and the Haynesville shales based on bed-by-bed estimates of total porosity, volumetric concentrations of kerogen and minerals, and fluid saturations from nonlinear joint inversion of conventional well logs. This technique showed that well logs can be applied to perform rock classification in organic-rich shale.

Gamero-Diaz et al. (2013) introduced a rock classification method that takes into account volumetric concentrations of minerals. The authors used a combination of core- and log-based mineralogical relationships to classify the following three primary groups: siliceous mudstone, carbonate-rich mudstone, and argillaceous mudstone. Further work determined the sub-classes based on the relative mineral concentration in these three groups. A unique relationship between lithofacies and elastic properties (bulk and shear moduli) was discovered within the Horn River Basin formation, and researchers applied this relationship to invert directly the lithofacies from acoustic logs (Potma 2013). None of the rock classifications performed in organic- rich formations include elastic properties, which are important factors to determine the capability of the rock to be fractured. This factor must be considered when selecting production intervals in organic-shale reservoirs (Jarvie 2007; Mullen 2010; Britt and Schoeffler 2009).

1.2 Statement of the problem

Parameters conventionally used for sweet-spot selection, such as hydrocarbon content and porosity, are not sufficient in organic- rich formations. It is possible to have a

well with a good porosity and a high hydrocarbon content but minimal hydrocarbon production due to hydraulic fracture failure (Gupta et al. 2012). Since fracture stimulation is such an important part of the production and completion process in these reservoirs, rock mechanical properties and mineralogy must be taken into account when optimizing the well completion design. Furthermore, a brittle organic- rich formation is likely to be naturally fractured and respond in a positive manner to fracture stimulation, whereas a ductile formation might not be capable of maintaining a fracture. Hence, production from ductile formations is extremely challenging and uneconomical.

Rock mechanical properties, Young's Modulus and Poisson's Ratio in particular, and the mineralogy of the formation provide valuable information regarding brittleness of the formation and its fracture treatment potential; therefore, these properties must be taken into account when determining production intervals.

Rock classification proves powerful when selecting the best production intervals. This thesis introduces a well-log-based rock classification method for organic-rich shale reservoirs that takes into account well-log-based estimates of petrophysical, compositional, and elastic properties of the formation. The first part of the thesis applies well logs and core measurements in an integrated interpretation to estimate water saturation, porosity, and volumetric concentrations of minerals to field examples in two formations the Haynesville shale and one in the Woodford shale. Then, effective medium models facilitated the assessment of elastic properties in both formations. The results from five models used to estimate elastic properties were compared to core measurements to determine which model provides the most accurate results when compared to laboratory

tri-axial core measurements. Finally, well-log-based estimates of petrophysical, compositional, and elastic properties, as well as direct application of well logs, served as inputs for rock classification.

1.3 Research objectives

The main objective of this thesis is to develop a reliable petrophysical rock classification method in organic-rich shale using well logs. Implementing an efficient rock classification using well logs improves (a) petrophysical evaluation of organic shale reservoirs, (b) fluid flow characterization, (c) detection of productive zones for fracturing jobs, and (d) prediction of fracturing and stimulation performances. An advantage that well-log-based rock classification has over conventional core-based methods is the capability to provide faster evaluation. Moreover, this approach provides depth-by-depth petrophysical and compositional evaluation for the entire well, not just at selected intervals, as in core-based experiments. The depth-by-depth evaluation of the formation increases the efficiency during operations, especially when selecting intervals to fracture.

The secondary objective of this thesis is to identify the most accurate effective medium method to estimate elastic properties in organic-rich shale using well logs. Assessment of elastic properties is an important step for successful rock classification because elastic properties impact the ability of the rock to start and maintain a fracture. To achieve this objective, five different models were applied to the three wells studied in this thesis to calculate bulk and shear modulus. Finally, this thesis compares laboratory

measurements of bulk and shear moduli to the results of the applied models to determine which one yields results with lowest relative error.

1.4 Outline of the thesis

Following this introductory section, Section 2 describes the method used in this research. Sections 3, 4, and 5 describe in detail how the method set forth in Section 2 was applied to two wells in the Haynesville shale and to one well in the Woodford shale. Finally, Section 6 summarizes the main findings of this thesis and presents final conclusions and suggestion for future work.

2. METHOD

2.1 Well-log interpretation

First, core X-Ray Diffraction (XRD) measurements highlighted existing minerals in the formation to delineate the compositional model for the formation. The determined compositional model includes non-clay minerals, clay minerals, organic matter, and total pore space (Ambrose et al. 2010; Quirein et al. 2010). Then, a joint inversion of the well logs determined compositional and petrophysical properties of the formation. The well logs used include photoelectric factor (PEF), bulk density, neutron porosity, compressional- and shear-wave slowness, and Elemental Capture Spectroscopy (ECS). TechLog (Mark of Schlumberger), a commercial multi-mineral solver, facilitated assessment of total porosity, water saturation, and volumetric/weight concentrations of minerals. Application of constraints based on XRD measurements and calculated volumetric concentration of kerogen minimized the non-uniqueness in the inversion process.

2.2 Assessment of elastic properties

Poisson's Ratio and Young's Modulus are two important mechanical properties to consider when developing an organic-rich shale where a fracturing job will most likely be necessary for economical production because they are chief indicators of a chosen zone's

sustainability for fracture treatment. Poisson's ratio corresponds to the ability of the matrix to fracture, and Young's modulus reflects the capability of the matrix to keep the fracture open (Rickman et al. 2008). To calculate Poisson's Ratio and Young's Modulus, researchers first estimate formation's effective bulk and shear moduli.

In this thesis, five models ranging from empirical rock-physics relationships to differential effective medium theories were applied to estimate bulk and shear moduli, as follows (a) empirical correlations based on acoustic-wave velocity measurements, (b) Backus Average, (c) SCA model, (d) DEM model, and (e) DEM-SCA combined method. Both the SCA and DEM models were applied using two different approaches, wet and dry, to make a total of seven distinct approaches. The inputs to these models include well logs, well-log-based calculated properties (e.g. volumetric concentrations of mineral components, porosity, and water saturation), the properties of the individual components of the matrix, and the geometric details of the shapes and spatial distributions of the components. Finally, the reliability of each of the five models chosen for the assessment of elastic moduli was investigated. The following sub-sections explain in detail the application of each of the five models.

2.2.1 Empirical correlations

An industry-standard technique to estimate the effective bulk and shear moduli directly from well logs is the application of V_p and V_s through the empirical correlations given by

$$V_p = \sqrt{\frac{K + \frac{4}{3}\mu}{\rho}} \tag{1}$$

and

$$V_s = \sqrt{\frac{\mu}{\rho}}, \tag{2}$$

where V_p is the compressional-wave velocity, V_s is the shear-wave velocity, μ is the shear modulus, K is the bulk modulus, and ρ is the bulk density of the saturated rock (Mavko et al. 2009). This model uses acoustic well logs (e.g. compressional- and shear-wave slowness) to determine the formation elastic properties. These approach do not provide the flexibility to model complex shales in terms of pore and grain shapes or compositions.

2.2.2 Backus Average

The Backus Average model was introduced to describe rock elastic moduli in layered media (Backus 1962). The Backus Average model is useful in layered formations where the rock mechanical behavior is transversely isotropic because it estimates the vertical and horizontal elastic moduli by taking into account volumetric concentrations of each rock constituent. For comparison reasons, this thesis only considers the vertical outputs for bulk and shear moduli. This model calculates the vertical properties by performing a weighted average using the volumetric concentrations of minerals and the individual mineral properties.

2.2.3 Self-Consistent Approximation (SCA)

The SCA is an inclusion-based model that represents the matrix grains and pores as idealized shapes. The model assumes that isolated mineral grains and pore inclusions with various aspect ratios in the rock are imbedded in an infinite background matrix of unknown properties (Mavko et al. 2009). The effective bulk and shear moduli of the rock are calculated by solving the coupled equations

$$\sum_{i=1}^{N} X_i (K_i - K_{SC}^*) P^{*i} = 0 \tag{3}$$

and

$$\sum_{i=1}^{N} X_i (\mu_i - \mu_{SC}^*) \mathrm{Q}^{*i} = 0, \tag{4}$$

where N is the total number of rock components, i refers to each of the individual rock components, X_i is the volumetric concentration of the rock component i, K_i and μ_i are bulk and shear moduli of the rock component i, respectively, and K^*_{sc} and μ^*_{sc} are the effective bulk and shear moduli of the rock, respectively. The factors P^*_i and Q^*_i correspond to the shape geometry of the rock component i (Berryman 1995).

This thesis research applied the SCA model using two different approaches. The first approach, which will be referred to as the "Wet SCA model," includes both fluids and minerals as inclusions of the rock when solving for K^*_{sc} and μ^*_{sc}. In the second approach, referred to herein as the "Dry SCA model," the SCA calculates dry bulk modulus of the formation by including only the minerals into the model when solving for K^*_{sc} and μ^*_{sc}. Then, to estimate the properties of the saturated rock, it is necessary to take into account the effect of the fluids. The Gassmann fluid substitution method (Gassmann

1951; Biot 1956) served this purpose. The Gassmann fluid substitution uses the following equations to transform the dry moduli into saturated moduli:

$$\frac{K_{sat}}{K_m - K_{sat}} = \frac{K_{dry}}{K_m - K_{dry}} + \frac{K_f}{\phi(K_m - K_f)} \tag{5}$$

and

$$\mu_{sat} = \mu_{dry}, \tag{6}$$

where K_{sat} is the saturated bulk modulus, K_{dry} is the dry bulk modulus (calculated K^*), K_m is the matrix bulk modulus, K_f is the pore-filling fluid bulk modulus, ϕ is the porosity and μ_{sat} is the saturated shear modulus. Both K_m and K_f were calculated from the properties of the individual components of the matrix.

The SCA model assumes that the mineral inclusion are idealized inclusion shapes. Furthermore, it assumes that the formation is isotropic, linear, and elastic.

2.2.4 Differential Effective Medium (DEM)

The DEM is an inclusion-based model that incrementally adds the mineral inclusions to a host matrix. This process assumes that each new mineral inclusion added to the model will displace the host matrix. This method not only takes into account the shapes of the added minerals and the final volume concentrations of the constituents, but also the order in which they are added.

The DEM method calculates the effective bulk and shear moduli K^*_{sc} and μ^*_{sc} by solving a system of coupled ordinary differential equations (Norris 1989; Zimmerman 1991b; Mavko et al. 2009; Berryman et al. 1992) given by

$$(1-y)\frac{d}{dy}\left[K^*(y)\right]=(K_i-K^*)P^{(*i)}(y) \tag{7}$$

and

$$(1-y)\frac{d}{dy}\left[\mu^*(y)\right]=(\mu_i-\mu^*)\mathrm{Q}^{(*i)}(y), \tag{8}$$

where y is the volumetric concentration of the rock component i, K_i and μ_i are bulk and shear moduli for the rock component i, respectively, and K^* and μ^* are the effective bulk and shear moduli of the rock, respectively. The factors P_i^* and Q_i^* correspond to the shape geometry of the rock component i (Berryman 1995).

Similar to the SCA model, the DEM model was used in two different approaches in this thesis. As a first approach, the "Wet DEM model," the fluids in the formation, along with the different minerals, were considered as inclusions in the matrix to calculate the elastic properties of the saturated rock. Then, as a second approach, the "Dry DEM model," the properties of the dry matrix were calculated using the DEM model. Then, using Gassmann's fluid substitution (Gassmann 1951), the saturated bulk and shear moduli are calculated. Similarly to the SCA model, the DEM model assumes idealized ellipsoidal inclusion shapes and an isotropic, linear, and elastic formation. In the DEM model the process of incrementally adding inclusions to the matrix is a thought experiment and should not be taken to provide an accurate description of the true evolution of rock porosity (Mavko et al. 2009).

2.2.5 SCA-DEM combination

Finally, a combined SCA and DEM model, introduced by Hornby et al. (1994), was investigated for the assessment of elastic moduli. This model first creates a host material that includes a host mineral and porosity using **Equations 3 and 4** from the SCA model. Then, to calculate the effective bulk and shear moduli of the rock, small volumes of the host matrix are removed and replaced by the other components of the matrix using **Equations 7 and 8** from DEM model. As in the stand-alone DEM model, the order in which the minerals are replaced will have an impact in the final result. Finally, the matrix, including all the components, is built. Gassmann's substitution (Gassmann 1951) incorporates the water and hydrocarbon saturations to obtain the bulk and shear moduli of the saturated rock. Since this model is a combination of the SCA and the DEM models the assumptions of ellipsoidal inclusion shapes and an isotropic, linear, and elastic formation remain for this model.

2.2.6 Young's Modulus and Poison's Ratio

From the previously calculated bulk and shear moduli, Young's Modulus *"E"* and Poisson's Ratio *"v"* can be calculates using **Equations 9 and 10**, respectively, as follows:

$$E = \frac{9K\mu}{3K - \mu} \tag{9}$$

and

$$v = \frac{3K - 2\mu}{2(3K + \mu)}, \tag{10}$$

where K and μ are the calculated bulk and shear moduli, respectively. Young's Modulus *"E"* and Poisson's Ratio *"v"* are correlated with the ability of a formation to start and maintain a fracture.

2.3 Brittleness index

The brittleness index determines the more likely intervals of the formation to successfully fracture based on Young's Modulus and Poisson's Ratio. Knowing this variable can be useful when determining which intervals to complete with a horizontal well, since a brittle rock is more likely to successfully fracture than a ductile rock (Gupta et al. 2012; Jarvie et al. 2007; Rickman et al. 2008). The rock brittleness is calculated using the previously calculated Young's Modulus and Poisson's Ratio with a model introduced by Rickman et al. (2008). One of the advantages of using well-log-based calculation of elastic properties over core measurements is that it is more common to have well logs across the entire interval of interest as well as the bounding rock layers (Rickman et al. 2008)

The effect of Young's Modulus and Poisson's Ratio on the brittleness is not similar; therefore they are unitized using their maximum and minimum values by the following equations:

$$E_{Britt} = \frac{E - E_{\min}}{E_{\max} - E_{\min}} \tag{11}$$

and

$$\upsilon_{Britt} = \frac{\upsilon - \upsilon_{\max}}{\upsilon_{\min} - \upsilon_{\max}}, \tag{12}$$

where E_{max} and E_{min} are the maximum and the minimum Young's Moduli, respectively, and υ_{max} and υ_{min} are the maximum and the minimum Poisson's Ratios, respectively. E_{Britt} and υ_{Britt} are the unitized Young's Modulus and Poisson's Ratio, respectively. Finally, the brittleness index is calculated via

$$Britt_{Index} = \left(\frac{E_{Britt} + \upsilon_{Britt}}{2} \right) 100 \ , \tag{13}$$

where $Britt_{Index}$ is the brittleness index expressed as a percent. Brittleness index is distinct to each well; therefore it is necessary to be careful when comparing two different wells. A 60% brittleness index in one well can be distinct from a 60% brittleness index in a different well, depending on the variation of the parameters in each well.

2.4 Rock classification

An unsupervised artificial neural network determined the different rock classes in the formations studied in this thesis. An unsupervised neural network creates a Self-Organizing Map (SOM), also known as Kohonen map, to classify the input data into different clusters or categories. The SOM takes the input data and classifies it under a chosen number of neurons equal to the desired number of clusters (Kohonen 1989). Each

of these neurons competes for each individual input data point; the neuron that resembles that input the most wins and the data point is moved closer to the winning neuron. After multiple iterations, the neural network SOM stabilizes with each neuron at the center of its cluster (Saggaf et al. 2001). Then, to finally classify the data points into categories, the unsupervised neural network requires a cluster analysis algorithm. In this thesis, the fuzzy clustering algorithm was used. Fuzzy clustering allows the different data points to belong to more than one cluster with different levels of membership. This process allows data points on the edge of two clusters to belong to both of them instead of forcing them to belong to one cluster or the other; the algorithm assigns a level of belonging between 0 and 1 to the data point and assigns it to the cluster with the highest level of belonging.

This thesis applies two separate rock classifications with two forms of input; the first one uses well logs as inputs, whereas the second one uses well-log-based estimates of petrophysical, compositional, and elastic properties as inputs. The artificial neural network ultimately defines the rock classes as a final output.

3. ASSESSMENT OF PETROPHYSICAL AND COMPOSITIONAL PROPERTIES

This section describes how I applied the method described in Section 2.1 to three field examples including two wells in the Haynesville shale and one well in the Woodford shale. The petrophysical evaluation contributed to calculate the volumetric concentrations of minerals, TOC concentration (wt. %), porosity, and water and hydrocarbon saturations in each field example. Core measurements served to validate and calibrate the petrophysical models.

3.1 Introduction

A well-log interpretation was performed on field datasets acquired from three different wells. The first well (Well No. 1) is located in the Eastern region of the Haynesville shale, the second well (Well No. 2) is located in the Western region of the Haynesville shale, and the third well (Well No. 3) is located in the Woodford shale in Oklahoma. For the rest of this thesis, these wells will be referred to as follows: Well No.1, Well No. 2, and Well No. 3, respectively.

The joint well-log interpretation included photoelectric factor (PEF), apparent resistivity, neutron porosity, bulk density, and Elemental Capture Spectroscopy (ECS) well logs, and core measurements to estimate petrophysical and compositional properties of the formation. XRD measurements served as the basis for determining the matrix

components. Grouping minerals with similar properties together minimized the number of unknown parameters, and, consequently, the non-uniqueness of the results. The matrix mineral components consisted of clay minerals, non-clay minerals, organic content, gas, and water. The organic matter was calculated as TOC weight concentration and then converted into volumetric concentration of kerogen by taking into account the organic maturity of the formation (Passey et al. 1990; Quirein et al. 2010). To further decrease the non-uniqueness of the results from the joint inversion of well logs, the following two constraints refined the well-log inversion (1) a pre- calculated volumetric concentration of kerogen and (2) a correlation of weight concentrations between different minerals based on XRD measurements. The resulting outputs of the joint inversion included estimates of porosity, fluid saturations, and volumetric concentrations of clay and non-clay minerals in all three wells studied.

3.2 An introduction to geology of the Haynesville shale and Woodford shales

3.2.1 The Haynesville shale

The upper Jurassic organic-rich Haynesville shale is currently one of the most productive shale-gas plays in the United States (Hammes et al. 2011). It extends through part of northeast Texas and northwest Louisiana and is surrounded by the Bossier formation from above and Smackover limestone from below. The Haynesville shale is composed of clay, organic matter, siliceous silt, and carbonates. Although the carbonate fraction is mainly calcite, in certain layers, calcite is replaced by dolomite, resulting in

dolomite being the dominant carbonate mineral. The porosity in this formation ranges from 8% - 12% and TOC varies from 1% - 8.5% (Hammes et al. 2011). The carbonate-rich facies contain TOC concentrations (wt.%) of under 2%. Organic matter is predominantly type II/III kerogen, with an average thermal maturity of 1.25% Ro (vitrinite reflectance). Development of the Haynesville shale challenges operators because of its highly laminated nature and heterogeneity of reservoir properties.

3.2.2 The Woodford shale

The upper Devonian Woodford shale is located in Oklahoma in the Anadarko basin. It extends from Dewey County to the southwest into Caddo County and northwest into Blaine and Dewey counties. Most of the Anadarko play lies in Canadian County, Oklahoma, hence the name Woodford shale.

The Woodford shale contains abundant marine organic matter and biogenic silica (Comer 2008; Kvale and Coffrey 2010). The true vertical depth ranges from 10,500 ft. (3,200 m), in the north east to 15,400 ft. (4,694 m) in the south west, with shales ranging from 100-300 ft. (30.5-91.5 m). The gas or condensate window in the Woodford shale occurs between 1.1 and 1.4 vitrine reflectance (Cardott 2010). The porosity ranges from 2% - 10%, and the TOC varies from 0% - 14% (Gupta et al. 2012). The Woodford shale features a complex structural geology and mineralogy, which makes horizontal drilling a slow process that wears out bits quickly.

3.3 Compositional and petrophysical model

This research applied Core X-Ray Diffraction (XRD) to define the minerals present in the different formations and determine the compositional models. The following two procedures reduced the number of unknowns in the model: (1) minerals with similar physical properties (e.g. illite-smectite, mixed-layer clay, and pure illite) were grouped as one unknown, (2) minerals with less than 2.5% volumetric concentration were removed from the model because the challenge on accurately estimating mineral concentrations that low using multi-mineral inversion. The final minerals in the compositional model included non-clay minerals (calcite, dolomite, feldspar, quartz, and pyrite), clay minerals (chlorite and illite), kerogen, and liquids (gas and water) (**Figure 1)**. The same compositional model was applied for all three wells.

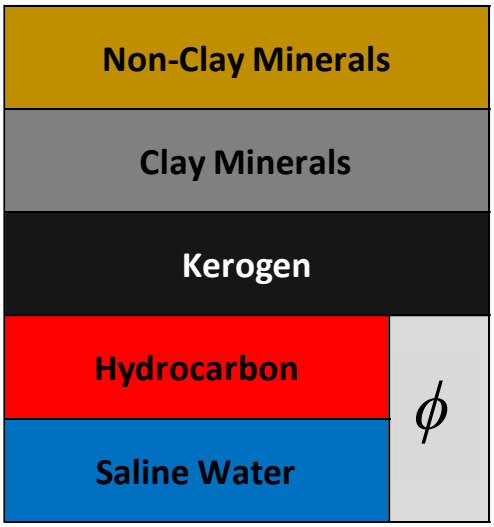

Figure 1: Assumed compositional model used for the well-log interpretation.

To minimize the non-uniqueness of the model, this research applied constraints based on linear correlations between minerals' XRD measurements. The applied constrains were distinct for each well.

The cross-plot between the volumetric concentration of plagioclase and quartz allowed for a linear correlation to be determined between these minerals that then served a constraint to the multi-mineral inversion. This correlation was found in both of the Haynesville shale wells. **Figures 2** and **3** show the results from the cross-plot and the regressions used as constraints in the multi-mineral analysis in Well No. 1 and Well No. 2, respectively.

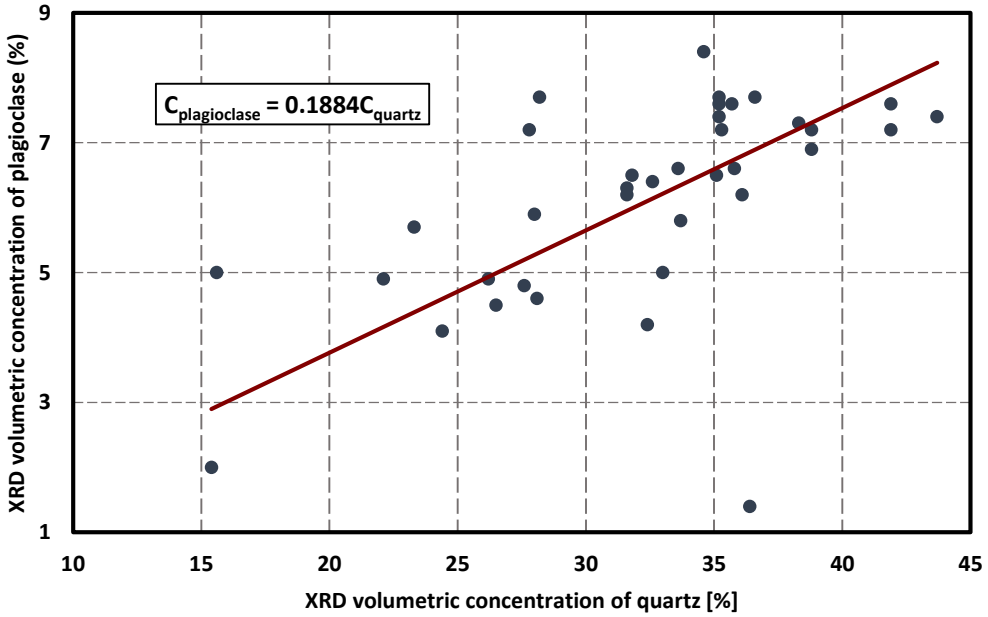

Figure 2: Correlation between the core XRD volumetric concentration of quartz and plagioclase in the Haynesville shale (Well No. 1).

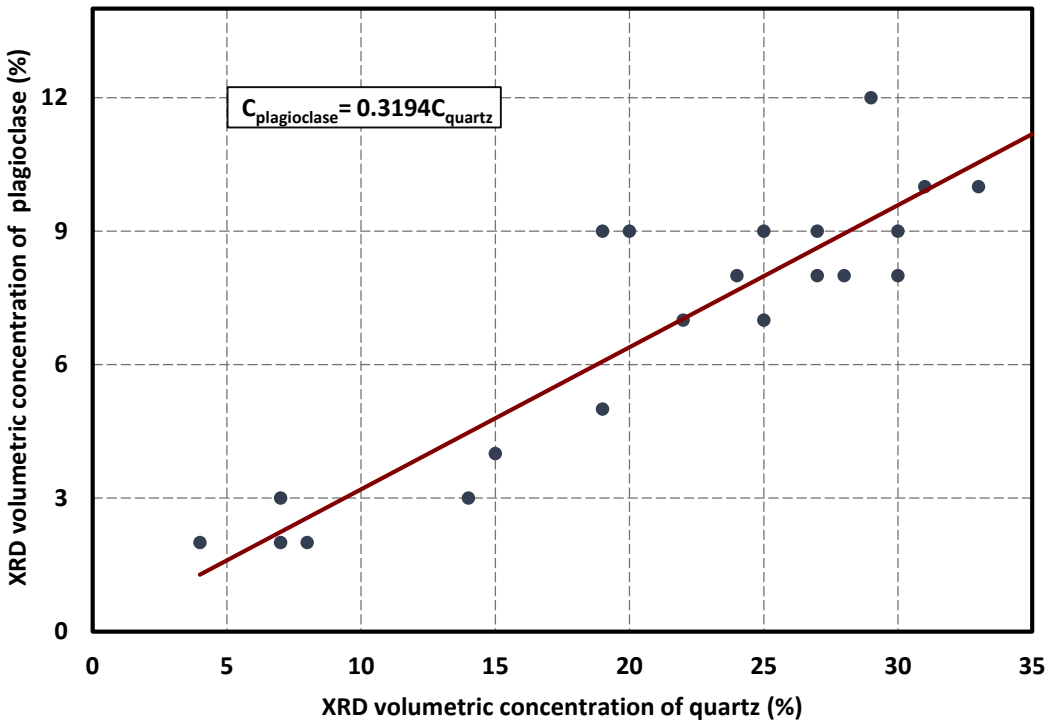

Figure 3: Correlation between the core XRD volumetric concentration of quartz and plagioclase in the Haynesville shale (Well No. 2).

A linear correlation between illite and chlorite occurred in both Well No.2 and Well No.3. **Figure 4 and 5** show, respectively, the results of the cross-plot and the regressions applied as constraints in the model. In the case of Well No. 3, four data points followed a different linear correlation. These four points belonged to an interval composed of over 50% volumetric concentration of illite vs. the 20% volumetric concentration of illite in the rest of the well interval.

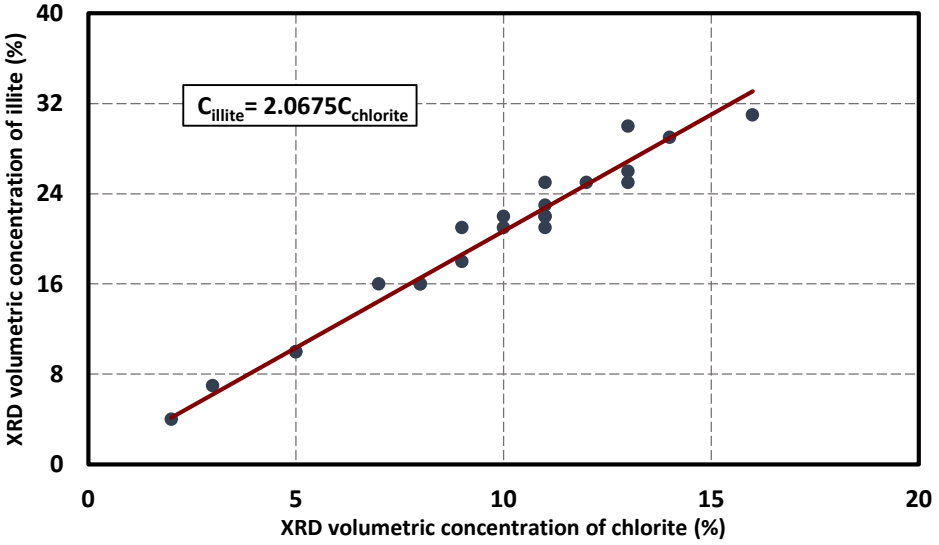

Figure 4: Correlation between the core XRD volumetric concentration of chlorite and illite in the Haynesville shale well (Well No. 2).

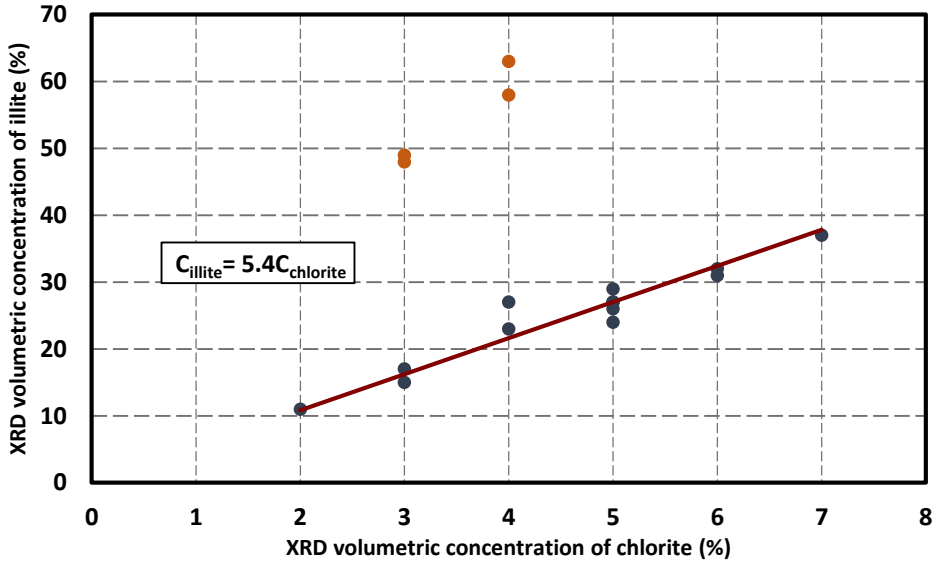

Figure 5: Correlation between the core XRD volumetric concentration of chlorite and illite in the Woodford shale well (Well No. 3).

3.4 Total Organic Content (TOC) calculation

A depth-by-depth TOC concentration (wt.%) was calculated for each well in this study. For both wells in the Haynesville shale Passey's Method (Passey et al. 1990) was used. On the other hand three different methods were used to estimate the TOC concentration (wt.%) in the Woodford shale (Well No. 3), because the conventional Passey's method may not be reliable due to the presence of high maturity kerogen in this well. The methods used in the Woodford shale well were (a) Passey's Method, (b) Density Correlation method, and (c) Uranium Correlation method.

3.4.1 Passey's method

This research applied Passey's method to calculate the TOC concentration (wt.%) in the Haynesville shale wells and as the first method to calculate the TOC concentration (wt.%) in the Woodford shale well. First, $\Delta logR$ was calculated using the compressional slowness and the deep resistivity logs by applying the formula

$$\Delta \mathrm{logR} = \log\left(\frac{R}{R_{baseline}}\right) + 0.02\ (\Delta t - \Delta t_{baseline}), \tag{14}$$

where R is the deep resistivity and Δt is the compressional-wave slowness. $R_{baseline}$ is the baseline of deep resistivity log measurements and $\Delta t_{baseline}$ is the baseline of compressional-wave slowness measurements. These baselines are determined in a non-source rock with minimal organic richness interval where both well-log curves overlap with. An overview of the Passey's method is shown in **Figure 6**.

Then, Equation 15 was used to calculate the-depth by-depth TOC,

$$TOC = C\left(\Delta \log \mathrm{R}\right) \times 10^{\left(2.297 - 0.1688 \times LOM\right)}, \tag{15}$$

where LOM is the level of organic metamorphism. C is called Passey's correction multiplier, it can be determined from core data. For both Well No. 1 and Well No. 2 in the Haynesville shale, this constant was assumed to be 1. On the other hand, because the kerogen in Well No. 3 in the Woodford shale is over mature, core measurements determined this constant to be 3.

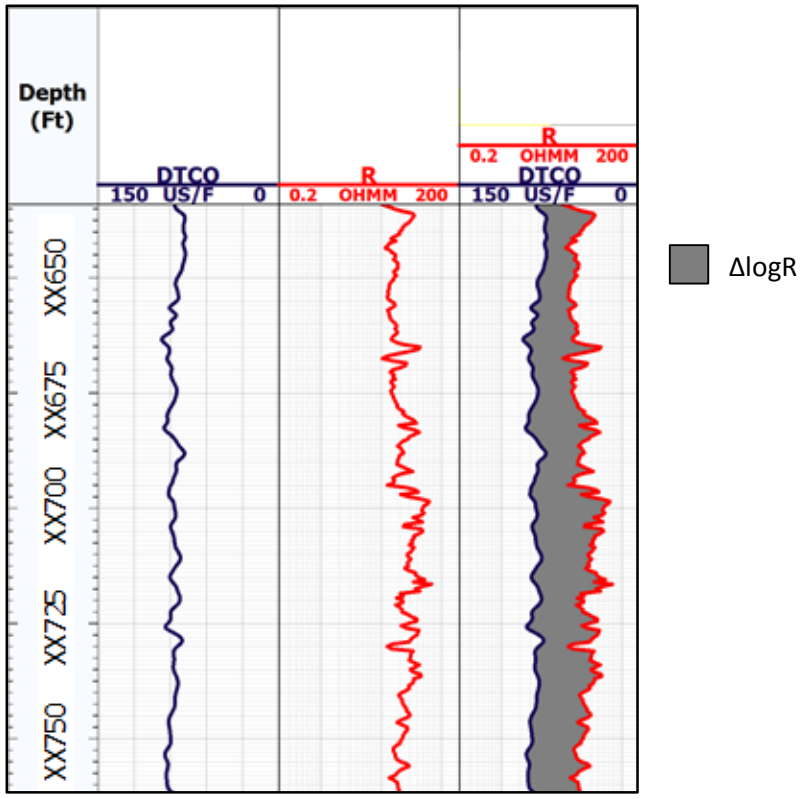

Figure 6: Field example of the ΔlogR method. Tracks from left to right include, Track 1: Depth, Track 2: Compressional slowness, Track 3: Apparent deep resistivity, and Track 4: Separation between the two curves (the gray shaded area) is the ΔlogR.

3.4.2 Density correlation method

The density correlation method, the second method applied to Well No. 3 in the Woodford shale, begins with the creation of a cross-plot between the core bulk density and the core TOC wt. %. Then, a linear regression to correlate these two properties the best given by **Equation 16** was found between the two properties.

$$TOC = -12.73\rho + 35.237, \tag{16}$$

where ρ is the core bulk density. **Figure 7** shows the cross-plot of bulk density vs. core TOC wt. % and the linear regression equation used to calculate TOC concentration (wt.%) in Well No. 3.

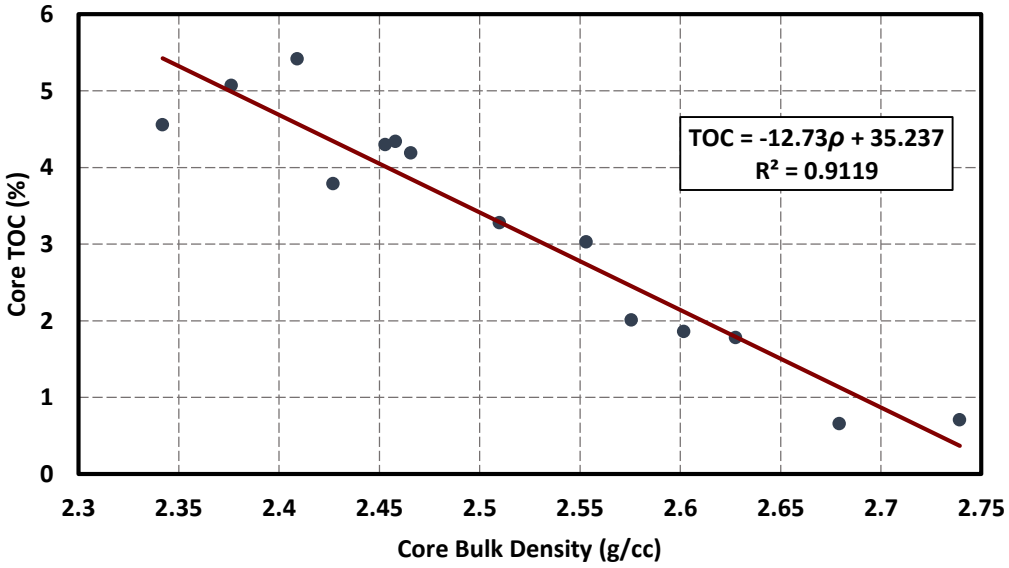

Figure 7: Core TOC vs. core bulk density cross-plot and linear regression used to find the correlation between both properties.

3.4.3 Uranium correlation method

The uranium correlation method served as the third method to calculate TOC in Well No. 3. A cross-plot between core TOC wt. % vs. uranium parts per million (ppm), obtained from the spectral gamma ray log, was generated. Then, as in the density method, a linear correlation occurred between these two properties. From this regression, the TOC was obtained in the well given by

$$TOC = 0.1485U + 1.1087 \, . \tag{17}$$

Figure 8 shows the cross-plot of the core TOC vs. uranium ppm and the linear regression used.

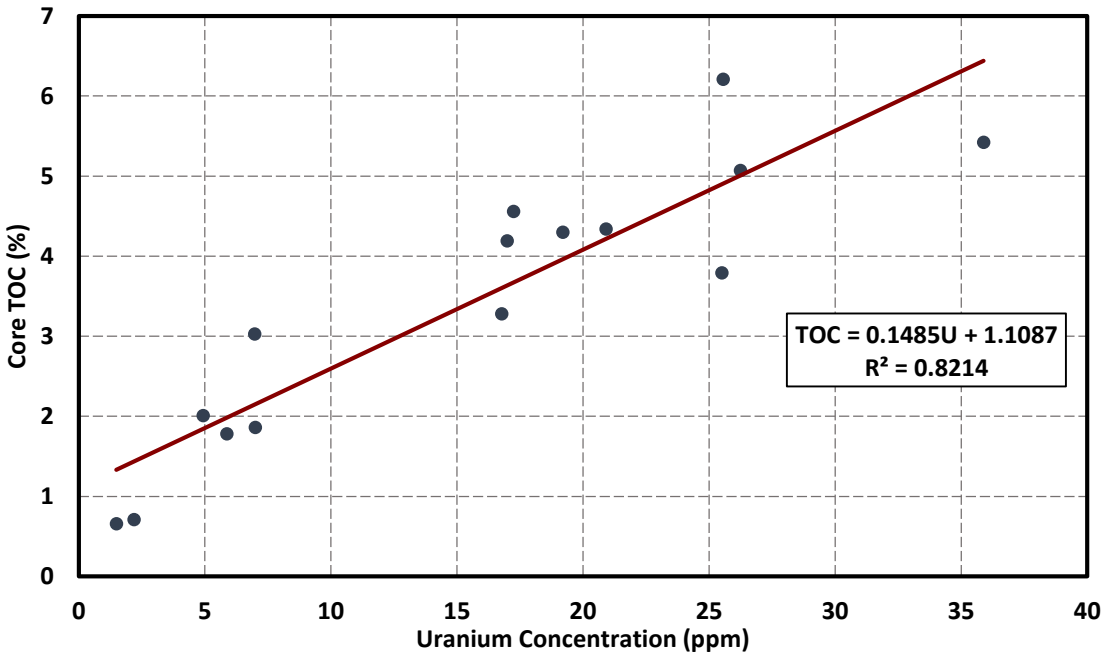

Figure 8: Core TOC vs. uranium concentration from spectral gamma ray cross-plot and linear regression used to find the correlation between both properties.

3.4.4 TOC method selection in the Woodford shale

Following the calculations of TOC concentration (wt.%) in Well No.3 using three distinct methods, this research compared the results against TOC concentration (wt.%) core measurement (**Figure 9**).

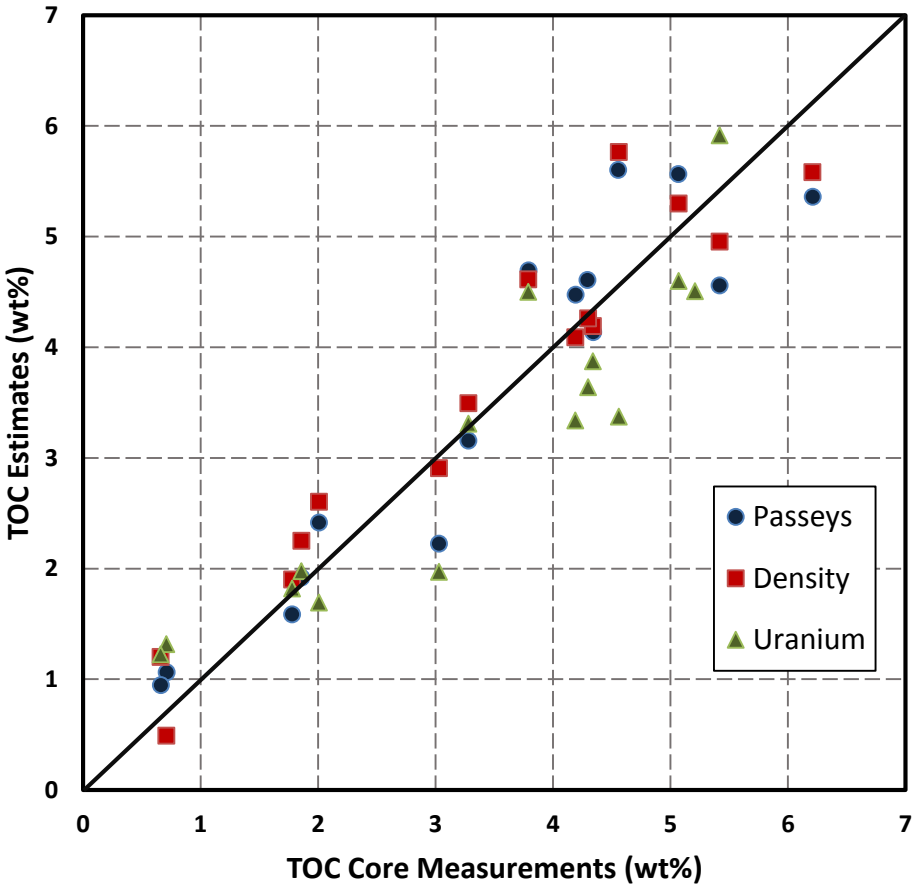

Figure 9: Comparison of Passey's, density, and uranium TOC models against core measurements.

This comparison revealed that the output from the Density Correlation method provides the most accurate results when the calculated TOC was compared to TOC obtained from laboratory core measurements with relative error under 9%. Therefore, this method takes precedence for the rest of this thesis.

Finally, after calculating the TOC concentration (wt.%) and validating it with core measurements in all three wells, the volumetric concentration of kerogen was calculated from the weight concentration of TOC. The volumetric concentration of kerogen served as a constraint in the multi-mineral analysis.

3.5 Multi-mineral analysis

Well-log inputs for the multi-mineral model, included conventional quad-combo and ECS logs. These well logs include Caliper, Gamma Ray (GR), apparent resistivity, bulk density, neutron porosity photoelectric factor (PEF), Compressional- and Shear-wave velocities, and ECS (**Figure 10).** The objective of this inversion was to obtain the volumetric concentrations minerals, the total porosity, and water saturation.

The model proved to be underdetermined; therefore, the solution given by the inversion was non-unique. To make the model evenly determined and reduce the non-uniqueness of the solution, two different sets of constraints were applied to the inversion model. First, the previously described plagioclase-quartz and the chlorite-illite constraints were applied to the each of the wells to which they applied. Then, the previously calculated volumetric concentration of kerogen was applied as a constraint for the inversion model.

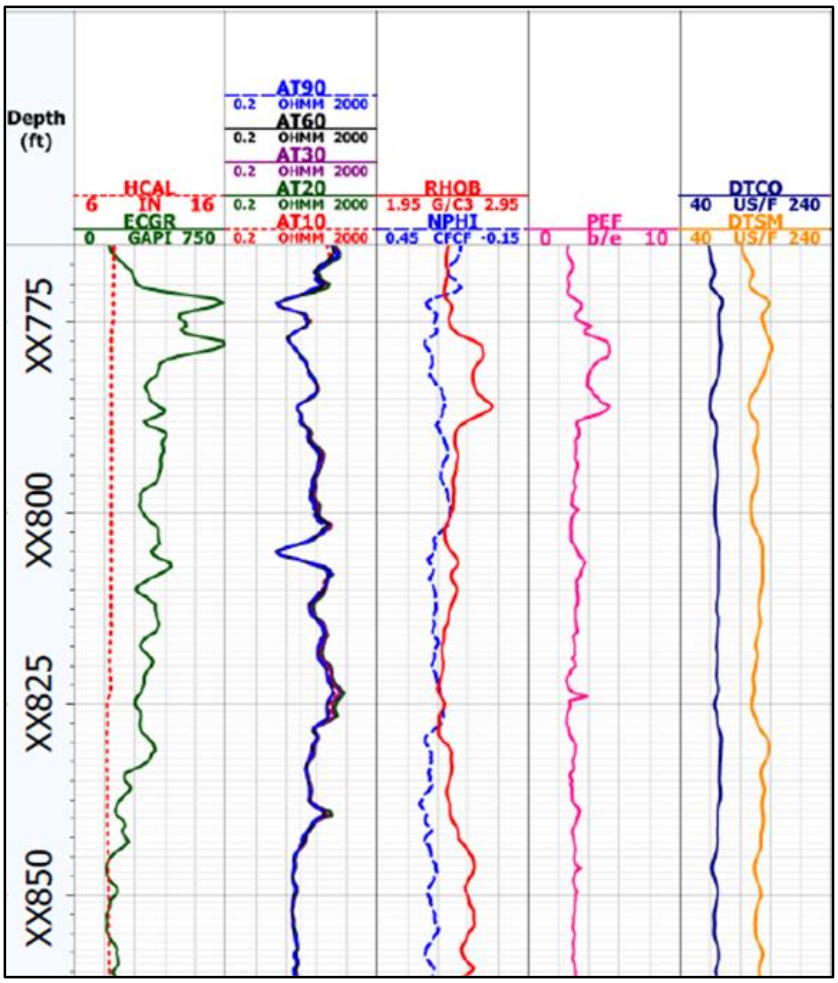

Figure 10: Example of the conventional quad-combo logs used in the three wells in this study. Tracks from left to right include, Track 1: Depth, Track 2: Gamma ray and caliper, Track 3: Apparent resistivity, and Track 4: Neutron porosity and bulk density, Track 5: Photoelectric factor, and Track 6: Shear- and compressional-wave slowness.

To calculate water saturations the multi-mineral analysis used the Dual Water model. This model was selected because the formations studied in this thesis contains clay bound water and this model accounts for effect of clay-bound water in the formation

(Clavier et al. 1984). **Tables 1 and 2** summarize the assumed Archie's parameters and fluid and formation properties used for well-log interpretation.

Table 1: Summary of assumed Archie's parameters and fluid and formation properties in the Haynesville shale.

Variable	Value	Units
Winsauer factor in Archie's equation, a	1.00	( )
Archie's porosity exponent, m	2.40	( )
Archie's saturation exponent, n	2.00	( )
Connate-water salt concentration	200	kppm, NaCl
In situ water density	1.05	g/cm^3
In situ gas density	0.19	g/cm^3
In situ kerogen density	1.3	g/cm^3
Formation temperature	132	°C

Table 2: Summary of assumed Archie's parameters and fluid and formation properties in the Woodford shale.

Variable	Value	Units
Winsauer factor in Archie's equation, a	1.00	( )
Archie's porosity exponent, m	1.67	( )
Archie's saturation exponent, n	2.15	( )
Connate-water salt concentration	160	kppm NaCl
In situ water density	1.0	g/cm^3
In situ gas density	0.1	g/cm^3
In situ kerogen density	1.3	g/cm^3
Formation temperature	105	°C

3.6 Results

This section presents the results from the multi-mineral analysis applied to the three wells. The multi-mineral analysis calculated TOC concentration (wt.%), water saturation, total porosity, and volumetric concentrations of minerals. The results for the two Haynesville shale wells (Well No.1 and Well No.2), and the Woodford shale (Well No.3) appear in **Figures 11, 12,** and **13,** respectively. Core data was also plotted along the results to validate each of the models. A comparison of the XRD core data (Track 11) and the outcomes of the multi-mineral inversion (Track 10) shows that the models accurately represent the mineralogy of the formation in all three cases. Furthermore, the estimates of TOC concentration (wt.%), water saturation, and total porosity (Tracks 7, 8, and 9, respectively) were plotted along core measurements for validation. The calculated average relative errors between core measurements and multi-mineral model outputs of TOC concentration (wt.%), water saturation, and total porosity in all three wells. The relative errors in estimates of TOC concentration (wt.%), water saturation, and total porosity were 10%, 9%, and 7%, respectively in Well No. 1, 10%, 9%, and 9%, respectively in Well No. 2, and 8%, 9%, and 10%, respectively, in Well No. 3

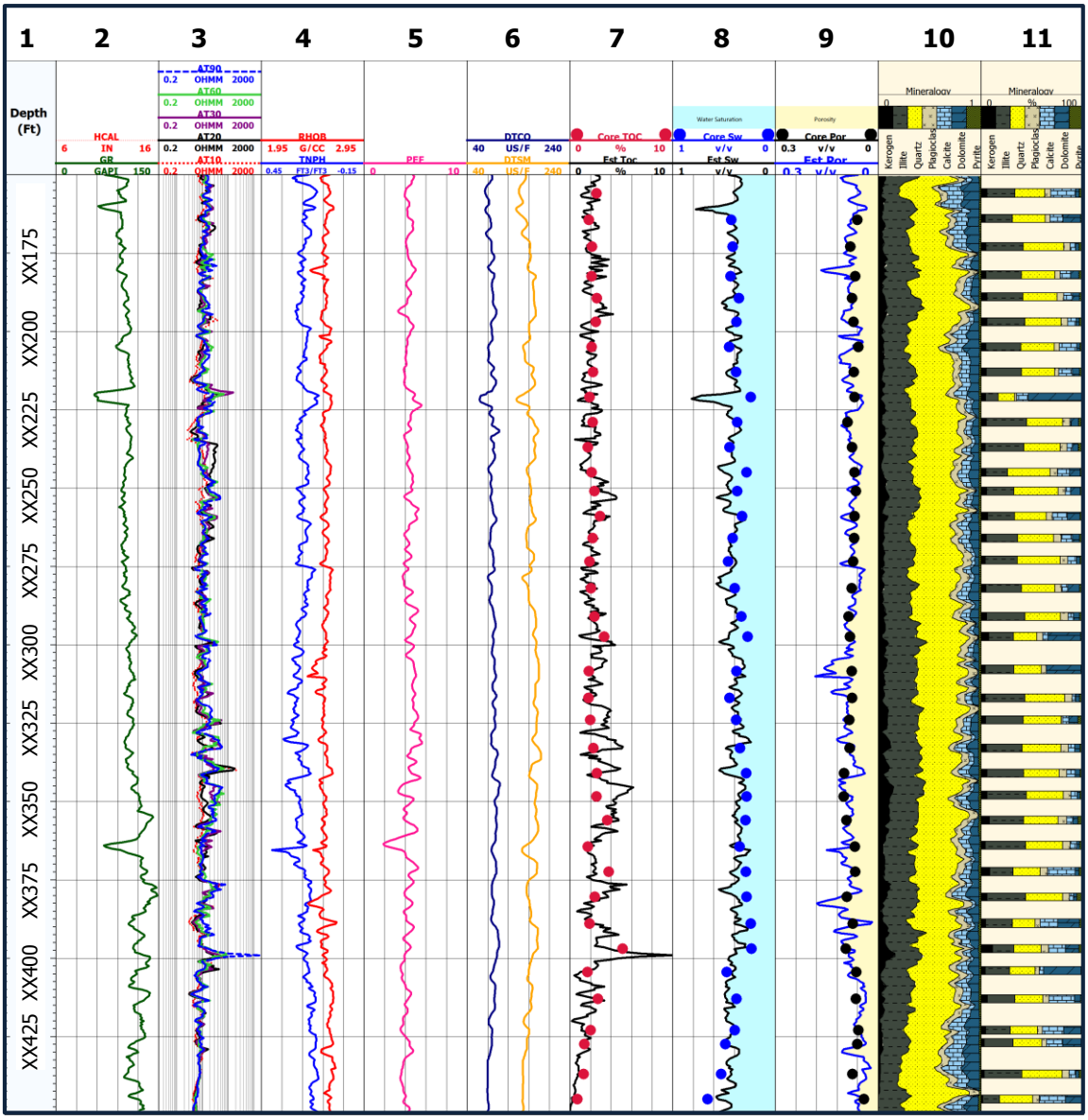

Figure 11: Conventional well logs and estimates of petrophysical and compositional properties in Well No. 1. Tracks from left to right include, Track 1: Depth; Tracks 2-6: Caliper gamma ray, apparent resistivity, neutron porosity (in water-filled limestone porosity units), bulk density, PEF, and shear- and compressional-wave slowness; Track 7-9: well-log-based estimates of water saturation and porosity, TOC, compared to the corresponding core measurements (blue, black, and red dots); Track 10: Volumetric concentrations of minerals calculated using well logs; Track 11: XRD core measurements.

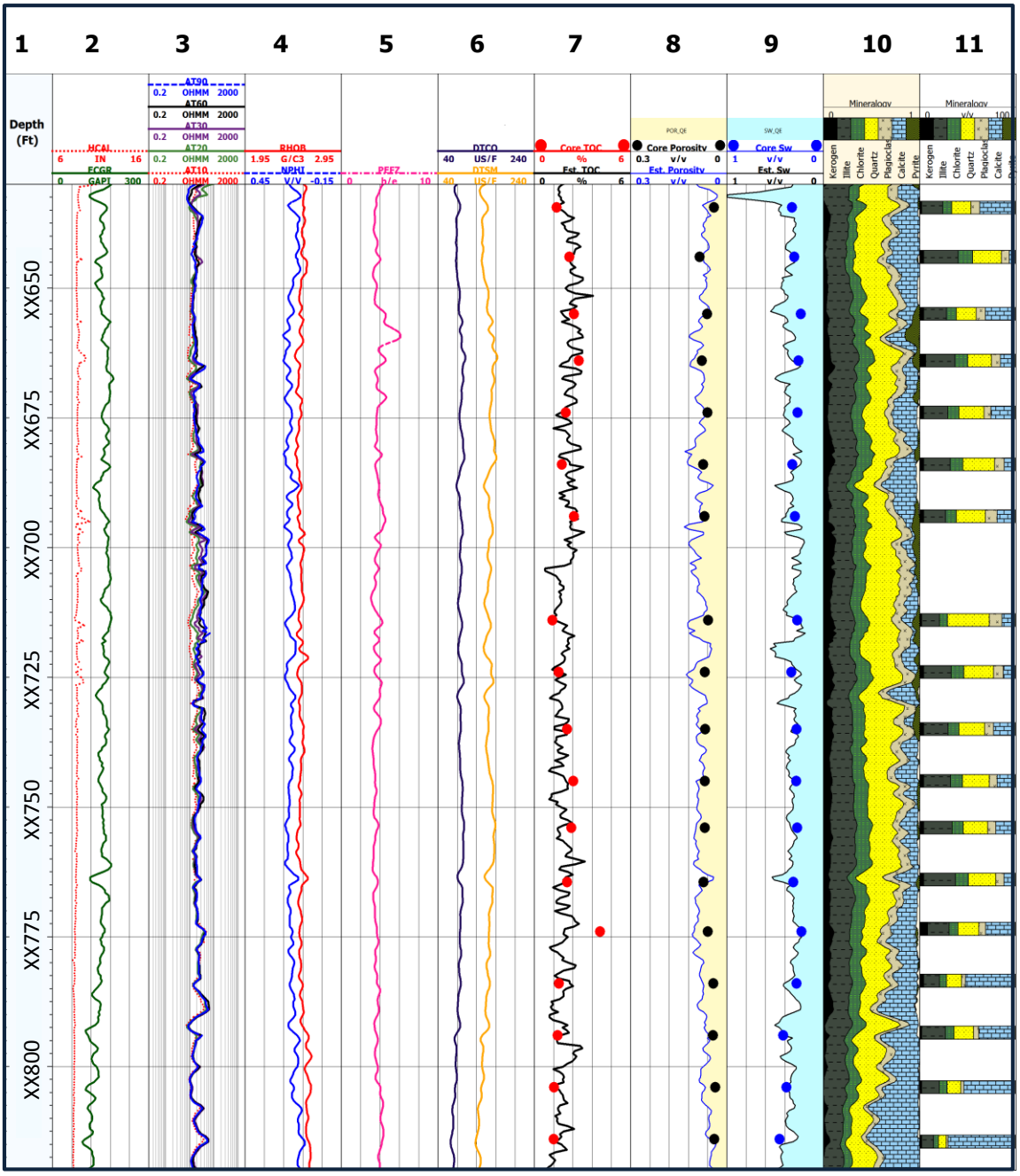

Figure 12: Conventional well logs and estimates of petrophysical and compositional properties in Well No. 2. Tracks from left to right include, Track 1: depth; Tracks 2-6: Caliper gamma ray, apparent resistivity, neutron porosity (in water-filled limestone porosity units), bulk density, PEF, and shear- and compressional-wave slowness; Track 7-9: Well-log-based estimates of water saturation and porosity, TOC, compared to the corresponding core measurements (blue, black, and red dots); Track 10: Volumetric concentrations of minerals calculated using well logs; Track 11: XRD core measurements.

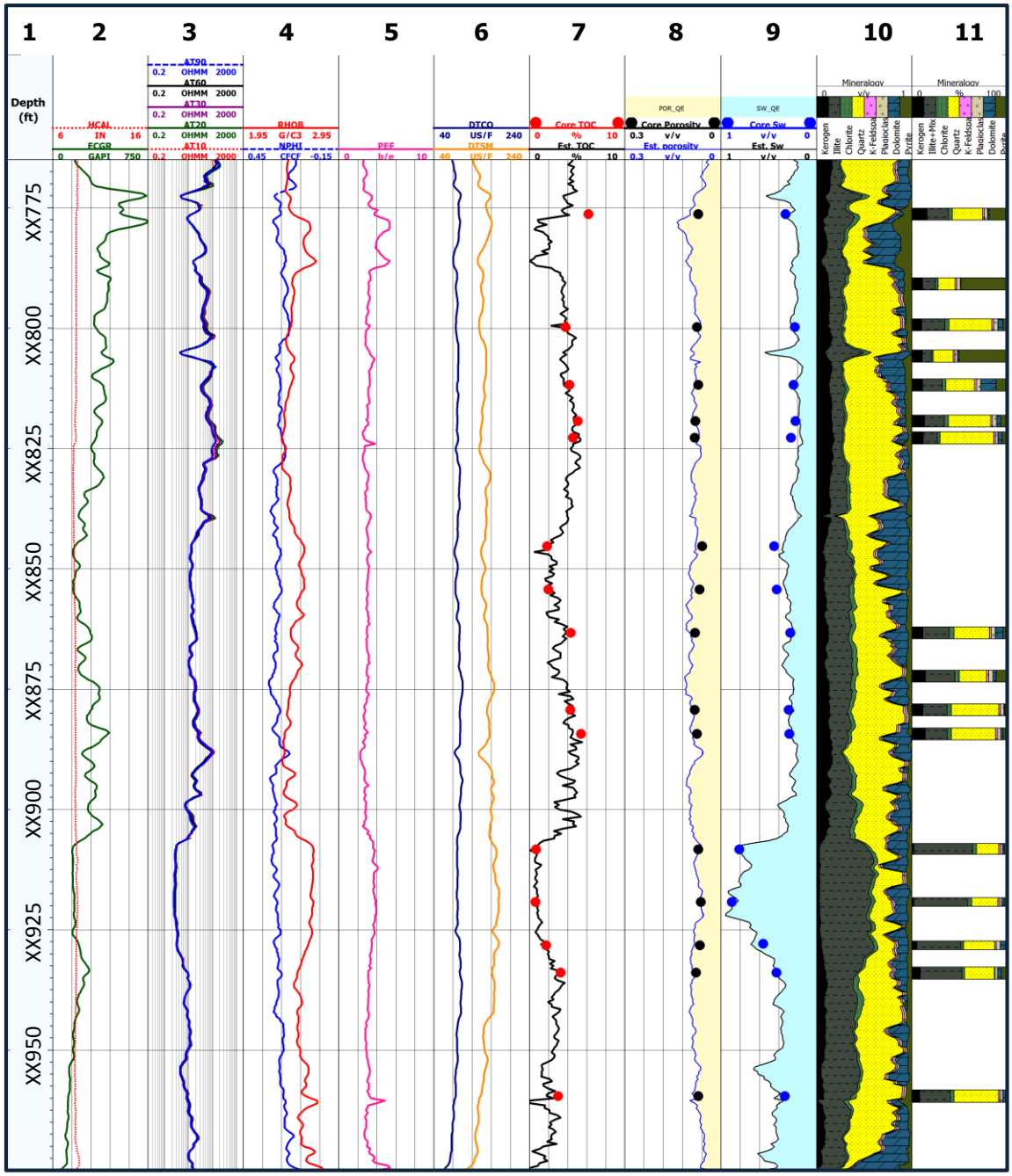

Figure 13: Conventional well logs and estimates of petrophysical and compositional properties in Well No. 3. Tracks from left to right include, Track 1: Depth; Tracks 2-6: Caliper gamma ray, apparent resistivity, neutron porosity (in water-filled limestone porosity units), bulk density, PEF, and shear- and compressional-wave slowness; Track 7-9: Well-log-based estimates of water saturation and porosity, TOC, compared to the corresponding core measurements (blue, black, and red dots); Track 10: Volumetric concentrations of minerals calculated using well logs; Track 11: XRD core measurements.

4. ASSESSMENT OF ELASTIC PROPERTIES

This section describes the application of the method set forth in Section 2.2 to all three wells. Calculated bulk and shear moduli were used to determine Young's Modulus and Poisson's ration, which subsequently were used to determine the depth-by-depth brittleness index in the three wells.

4.1 Assessment of well-log-based bulk and shear moduli

After developing the compositional and petrophysical model, and validating it with core measurements, the depth-by-depth effective bulk and shear moduli of the rock was approximated using: (a) empirical correlations based on acoustic-wave velocity measurements, (b) Backus Average, (c) SCA model, (d) DEM model, and (e) DEM-SCA combined method, each of these methods uses different properties as inputs. The empirical equations use the compressional- and shear- wave slowness measured by the quad-combo logging tools as input. The Backus Average, on the other hand, uses as inputs the volumetric concentrations of minerals and the individual mineral bulk and shear moduli of these minerals. *The Rock Physics Handbook* by Mavko et al. (2009) provided the individual mineral bulk and shear values, and the multi-mineral analysis described in Section 4 provided the volumetric concentrations of minerals. Finally, the SCA, DEM, and SCA-DEM combination, denominated inclusion-based models, use as inputs the

individual minerals bulk and shear moduli, the volumetric concentrations of minerals, and the geometric details of the shapes and spatial distributions of the mineral components.

The geometric shapes and the aspect ratios for each rock constituent for the inclusion-based models were set based on the observations of core Scanning Electron Microscope (SEM) images and previous geologic studies on the Haynesville shale (Curtis et al. 2010; Hammes et al. 2011). For stiffer rock components (e.g., quartz), spherical shapes were used. On the other hand, penny-crack shapes were assigned to the softer components (e.g., illite). The reservoir fluids were assumed to be present in penny-cracks or oval-shaped pores. All the minerals and fluid had only one assigned shape and aspect ratio with the exception of calcite which, after looking at the SEM images, it was determined that two shapes and aspect ratios were required to represent accurately the presence of calcite in these formations. **Tables 3 and 4** summarize the shapes and aspect ratios selected for each of the individual minerals.

Table 3: Mineral Inclusion Aspect Ratios

Calcite	Chlorite	Dolomite	Illite	Kerogen	Feldspar	Pyrite	Quartz
1/0.01	0.1	1	0.1	0.01	1	1	1

Table 4: Mineral Inclusion Geometrical Shapes

Calcite	Chlorite	Dolomite	Illite	Kerogen	Feldspar	Pyrite	Quartz
Sphere/Penny Crack	Sphere	Sphere	Penny Crack	Penny Crack	Sphere	Penny Crack	Sphere

4.2 Laboratory measurements

After estimating bulk and shear moduli using the selected models in all three wells, this research process carried out laboratory experiments to calculate mechanical properties. Core samples for tri-axial measurements were available in the both of the Haynesville shale wells. The tri-axial measurements were carried out using the GCTS Tri-axial System RTX-1500 shown (**Figure 14)** at the Rock Mechanics Laboratory in the Harold Vance Department of Petroleum Engineering at Texas A&M University. This system has an axial load capacity of 1500 kN, and a hydrostatic pressure capacity of 137 MPa; the hydrostatic pressure was provided by hydraulic oil DTE-25. The pore and overburden pressures in the Haynesville shale range from 65 - 70 MPa and 80 - 90 MPa, respectively.

Two different experimental procedures were performed under drained conditions and room temperature on core samples drilled perpendicularly to the vertical axis of symmetry in the Haynesville shale. This research, used a tri-axial rock system to calculate the bulk modulus. In this experiment, core plugs were loaded hydrostatically from an initial confining pressure of 5 MPa to 45 MPa, at a constant rate of 0.75 MPa/min. This pressure induced a volumetric change in the samples. Then, to determine bulk modulus, the slope that represents the rate of change of the confining pressure with respect to the volumetric strain was used, and is given by

$$K = \frac{\Delta \sigma_c^{'}}{\Delta \varepsilon_v}, \tag{18}$$

where K is the bulk modulus, σ'_c is the confining hydrostatic pressure, and ε_v is the volumetric strain.

Figure 14: Tri-axial system used to measure bulk and shear moduli in the laboratory.

A second set of experiments calculated shear modulus. For this case, the core samples were loaded under tri-axial conditions. Then, the samples were loaded uniaxially at a constant strain rate of 0.5 %/min, while the confining pressure was held constant. In this case, a constant hydrostatic pressure corresponding to the integrated pressure with depth and density was used. The core plugs were loaded up to a maximum axial strain of 0.25 mm/mm. From this experiment, the Young's Modulus measurement can be expressed by

$$E = \frac{\Delta S_d^{'}}{\Delta \varepsilon_a}, \tag{19}$$

where E is Young's Modulus, S_d is the deviatory stress, and ε_a is the axial strain. Finally, the obtained Young's Modulus was combined with the previously calculated bulk modulus and used to estimate shear modulus using the following expression:

$$\mu = \frac{3KE}{9K - E}, \tag{20}$$

where μ is Poisson's Ratio, E is Young's Modulus, and K is the previously calculated bulk modulus

The laboratory measurements of bulk and shear moduli were used to determine the accuracy of the different models to estimate elastic properties. The comparison allowed the selection of the most accurate model to estimate bulk and shear moduli in the formations studied.

4.3 Model comparison against core measurements

The estimates of bulk and shear moduli of both wells in the Haynesville shale (Well No.1 and Well No. 2) were compared against laboratory measurements to determine the most accurate model to estimate elastic properties in this formation. The shear modulus results of all seven approaches were compared to the laboratory shear modulus calculations. **Table 5** shows the relative error calculation between the calculated shear modulus and the laboratory core measurements in Well No.1 and Well No.2.

Table 5. Relative errors of the shear modulus estimates from different models compared to core measurements in Well No. 1 and Well No. 2

Model	Model results vs. core measurements relative error (%)	
	Well No.1	Well No.2
Backus Average shear modulus	64.8	33.7
Sonic logs empirical equations shear modulus	35.7	21.4
Wet Self-Consistent Approximation shear modulus	8.5	7.0
Dry Self-Consistent Approximation shear modulus	14.5	7.4
Wet Differential Effective Medium shear modulus	28.3	15.4
Dry Differential Effective Medium shear modulus	22.8	12.6
SCA-DEM combination shear modulus	12.6	8.0

Table 5 shows that the inclusion-based models have an outcome relative error at least 10% lower than the empirical equations and the Backus Average, when compared to

shear moduli core measurements. Empirical equations and the Backus Average show relative errors of up to 35% and 64%, respectively, when comparing them to shear modulus core measurements. Of the three inclusion-based models, the Wet SCA approximation shows the least relative error when estimating shear moduli, with average relative error of 8.5% and 7% in Well No. 1 and Well No. 2, respectively.

On the other hand, only the results from the SCA, DEM, and SCA-DEM combination models were compared to the core measurement because these models have the ability to estimate the dry bulk modulus of the rock and, since the laboratory experiments were performed under flushed conditions, comparison to dry properties was the most appropriate. **Table 6** shows the relative error calculation between the calculated bulk modulus and the calculated bulk modulus from laboratory measurements.

Table 6. Relative errors of the bulk modulus estimates from different models compared to core measurements in Well No. 1 and Well No. 2

Model	Model results vs. core measurements relative error (%)	
	Well No.1	Well No.2
Self-Consistent Approximation dry bulk modulus	9.8	12.4
Differential Effective Medium dry bulk modulus	11.7	17.2
SCA-DEM combination dry bulk modulus	13.3	15.3

The results appearing in **Table 6** show that, out of the three models compared against core measurements, the bulk modulus calculated using the SCA model yields the

smallest relative error of 9.8% in Well No.1 and 12.4% in Well No. 2. The comparison of the different approached to the laboratory core measurements determined the Wet SCA to be the most accurate model to estimate bulk and shear modulus in Well No.1 and Well No. 2.

The dataset from the Woodford shale (Well No.3) lacked core measurements of elastic properties; therefore the most accurate model to estimate elastic properties could not be determined. The bulk and shear moduli results from all seven approaches for both formations were compared to identify if they follow the same trend in both formations. The Dry SCA model was selected as the baseline model from this comparison.

Tables 7 and **8** show the results of the comparison for the bulk and shear moduli, respectively.

Table 7: Comparison of the bulk modulus results from different models to the dry self-consistent approximation bulk modulus in the three wells from the Haynesville shale and Woodford shales

Model	Model results vs. low-frequency SCA (%)		
	Well No.1	Well No.2	Well No.3
Backus Average bulk	36.3	51.2	23.5
Sonic logs empirical equations	18.6	22.4	23.0
Wet Self-Consistent Approximation	14.0	9.0	9.3
Wet Differential Effective Medium	18.5	18.9	19.5
Dry Differential Effective Medium	12.4	7.7	17.4
SCA-DEM combination	11.1	9.3	16.2

Table 8: Comparison of the shear modulus results from different models to the dry self-consistent approximation shear modulus in the three wells from the Haynesville shale and Woodford shales

Model	Model results vs. low-frequency SCA (%)		
	Well No.1	Well No.2	Well No.3
Backus Average	52.7	51.0	23.7
Sonic logs empirical equations	35.3	23.7	22.1
Wet Self-Consistent Approximation	7.1	3.8	4.4
Wet Differential Effective Medium	19.4	18.9	9.7
Dry Differential Effective Medium	14.9	15.5	6.4
SCA-DEM combination	13.0	7.2	5.1

The results from inclusion-based models are comparable to the selected baseline model; these models had a variability of up to 20% when compared to the baseline model. On the other hand, the results from the Backus Average and the empirical equations yield greater errors with results straying up to 52% from the baseline model. Because Well No. 3 lacked elastic bulk and shear measurements to compare the different models against this research used the Wet SCA model to calculate elastic properties in Well No. 3.

Using **Equations 9** and **10,** the results from the Wet SCA were used to calculate the Young's Modulus and Poisson's Ratio in each well. Finally, the Young's Modulus and Poisson's Ratio facilitated the calculation of the brittleness index of the formation.

4.4 Brittleness index

Calculating a rock brittleness index using well-log-based estimates of elastic properties helps determine the relative brittleness of the formation. The brittleness index is a function of two important measures of fracture effectiveness (a) fracture initiation potential in a rock (Young's Modulus) and (b) the capability of the rock to maintain a fracture (Poisson's Ratio) (Rickman et al. 2008). High values of Young's Modulus and low values of Poisson's Ratio indicate a brittle rock that enables successful hydraulic fracturing. Using the Young's Modulus and Poisson's Ratio results from Section 5.3 the brittleness index for all three wells was calculated.

Figure 14 shows the cross-plots of the brittleness index vs. Young's Modulus and Poisson's Ratio in (a) Haynesville shale (Well No.1), (b) Haynesville shale (Well No.2), and (c) Woodford shale (Well No.3). **Figure 14**, shows that the increase in Poisson's Ratio has a negative effect on the brittleness index and an increase in Young's Modulus has a positive effect on the brittleness of the formation. Therefore, intervals containing high Young's Modulus and low Poisson's Ratio should be targeted for hydraulic fracture completion.

The brittleness of the formation is also dependent on the mineralogy of the formation. **Figure 15** shows the impact on the brittleness index of the volumetric concentrations of quartz and illite in (a) Haynesville shale (Well No.1), (b) Haynesville shale (Well No.2), and (c) Woodford shale (Well No.3).

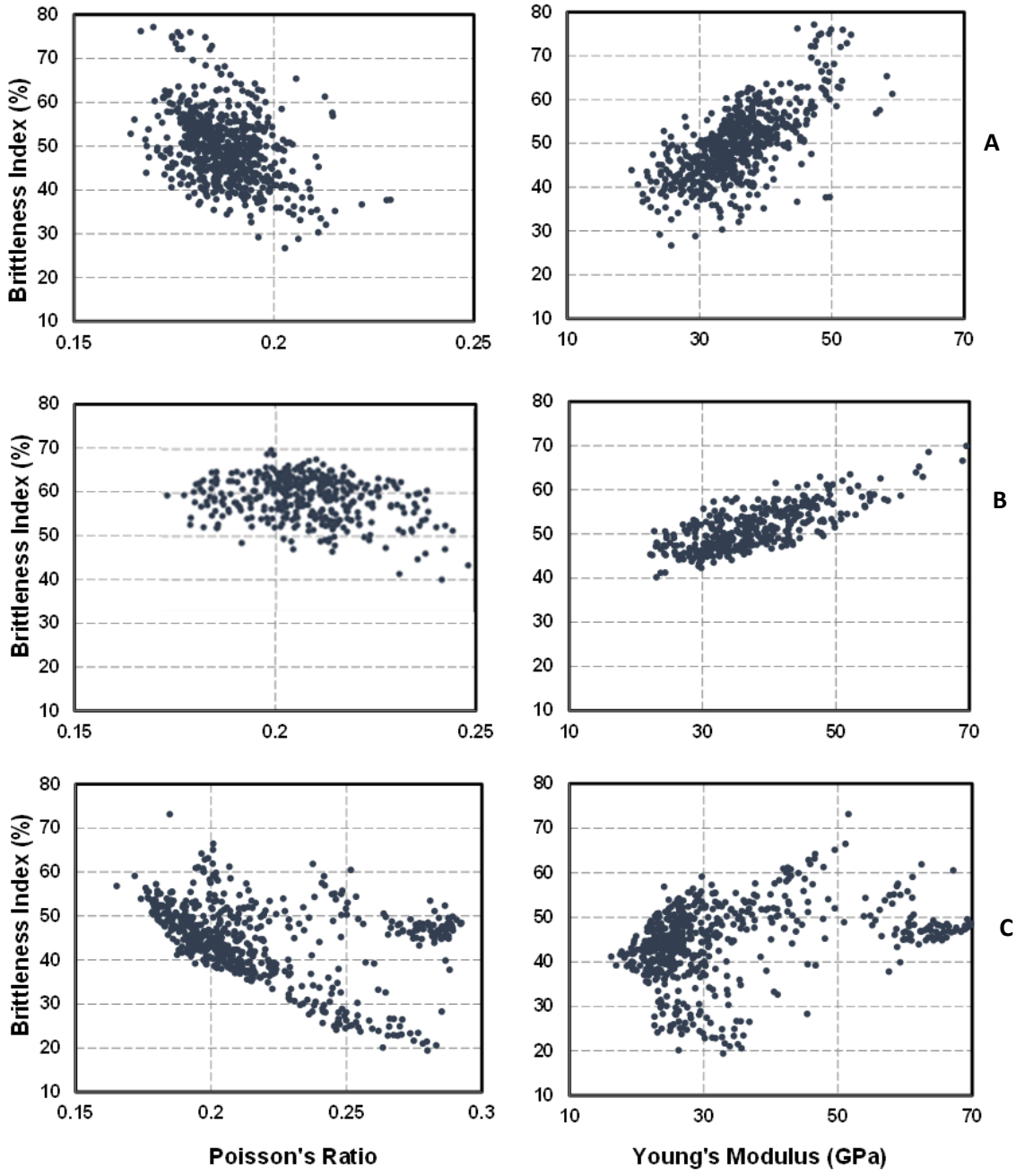

Figure 15: Brittleness index vs. Poisson's Ratio and Young's Modulus cross-plots in: (a) Haynesville shale well (Well No. 1), (b) Haynesville shale well (Well No. 2), and (c) Woodford shale well (Well No.3).

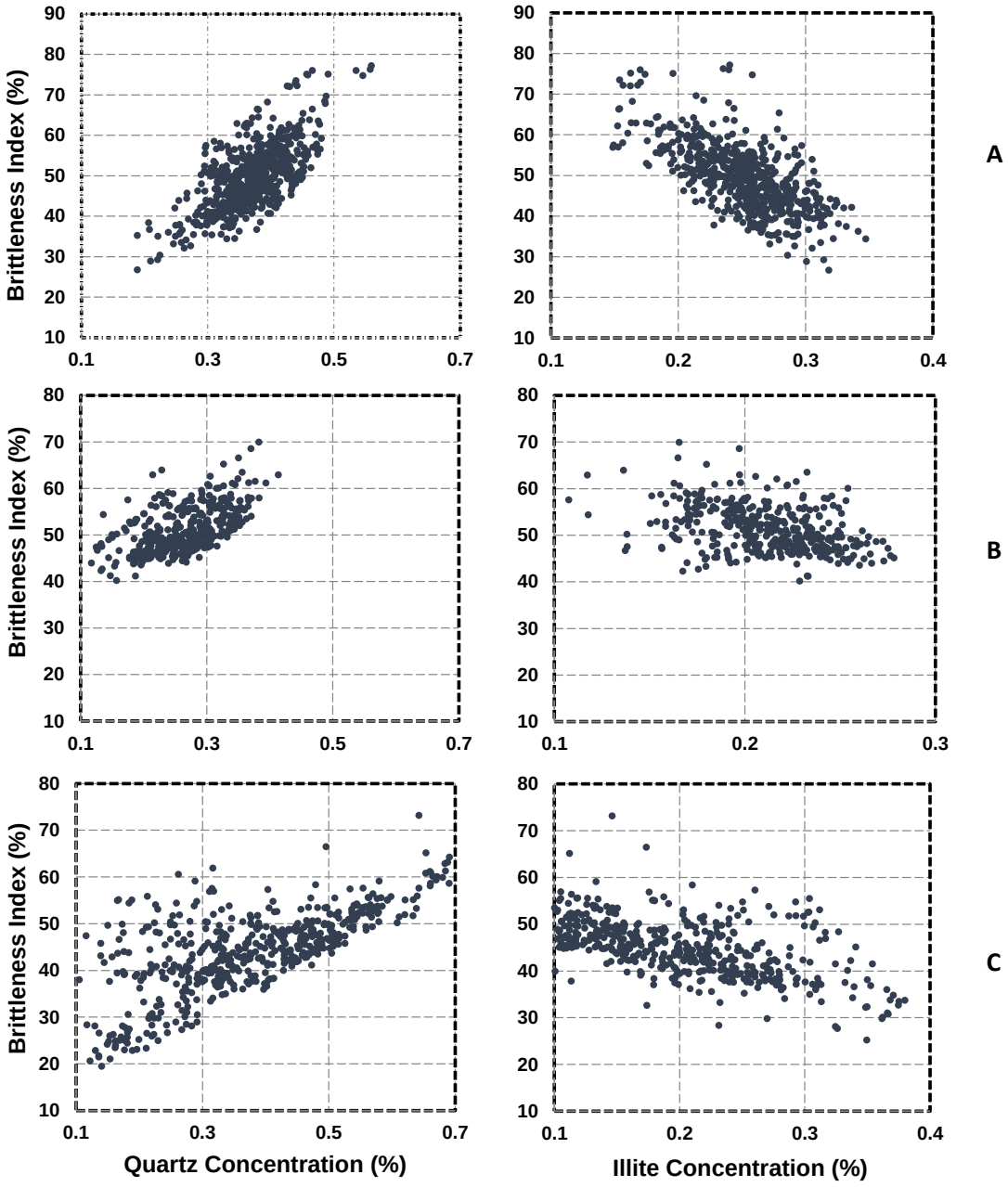

Figure 16: Brittleness index vs. volumetric concentration of quartz and illite cross-plots in: (a) Haynesville shale well (Well No. 1), (b) Haynesville shale well (Well No. 2), and (c) Woodford shale well (Well No.3).

Figure 15 displays that higher quartz concentration results in an increase in the formation brittleness, whereas an increase in illite concentration causes a reduction in the formation brittleness. Therefore, intervals containing elevated volumetric concentration of quartz are more likely to fracture successfully. The impact of calcite and dolomite concentrations on the brittleness in these formations was moderate, similar to their impact on brittleness that other researchers have found in the Woodford and the Barnett shales (Gupta et al. 2012; Jarvie et al. 2007; Rickman et al. 2008).

4.5 Discussion

Figures 17, 18, and **19** show the results of the calculated elastic properties, bulk modulus, shear modulus, Young's Modulus, Poisson's Ratio, and brittleness index, along with the conventional well logs and the calculated petrophysical properties, used in Well No. 1, Well No. 2, and Well No. 3, respectively.

On each of these well-log plots, Tracks 9 and 10 show the results of the estimates of bulk and shear moduli calculated using the Wet SCA model along with the results from the laboratory experiments. Track 11 shows the results of Young's Modulus displayed in purple and Poisson's, displayed in green. Finally, track 12 displays the relative brittleness index. The results from this section show the mechanical heterogeneity in all three wells. It can be observed that the brittleness of the formation changes abruptly by moving vertically a couple of feet. This vertical heterogeneity in the formation is the reason why it is important to include elastic properties when performing a rock classification.

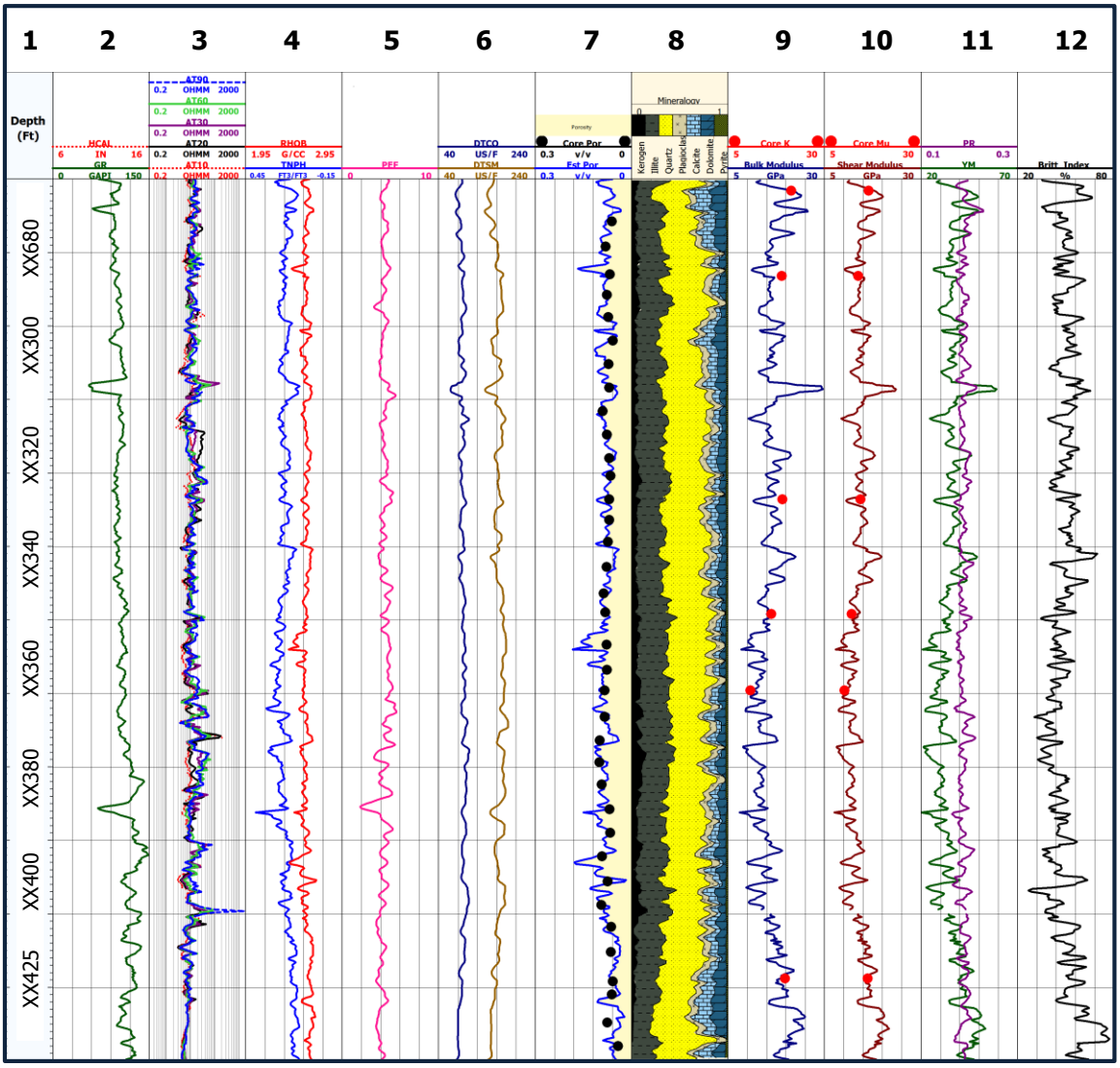

Figure 17: Conventional well logs and estimates of rock elastic properties in Well No 1. Tracks from left to right include, Track 1: Depth; Tracks 2-6: Caliper gamma ray, apparent resistivity, neutron porosity (in water-filled limestone porosity units), bulk density, PEF, and shear- and compressional-wave slowness; Track 7: Well-log-based estimate of porosity, Track 8: Volumetric concentrations of minerals calculated using well logs; Tracks 9-11: Well-log-based estimate of bulk modulus, shear modulus, Young's Modulus and Poisson's Ratio. Track 12: Calculated brittleness index.

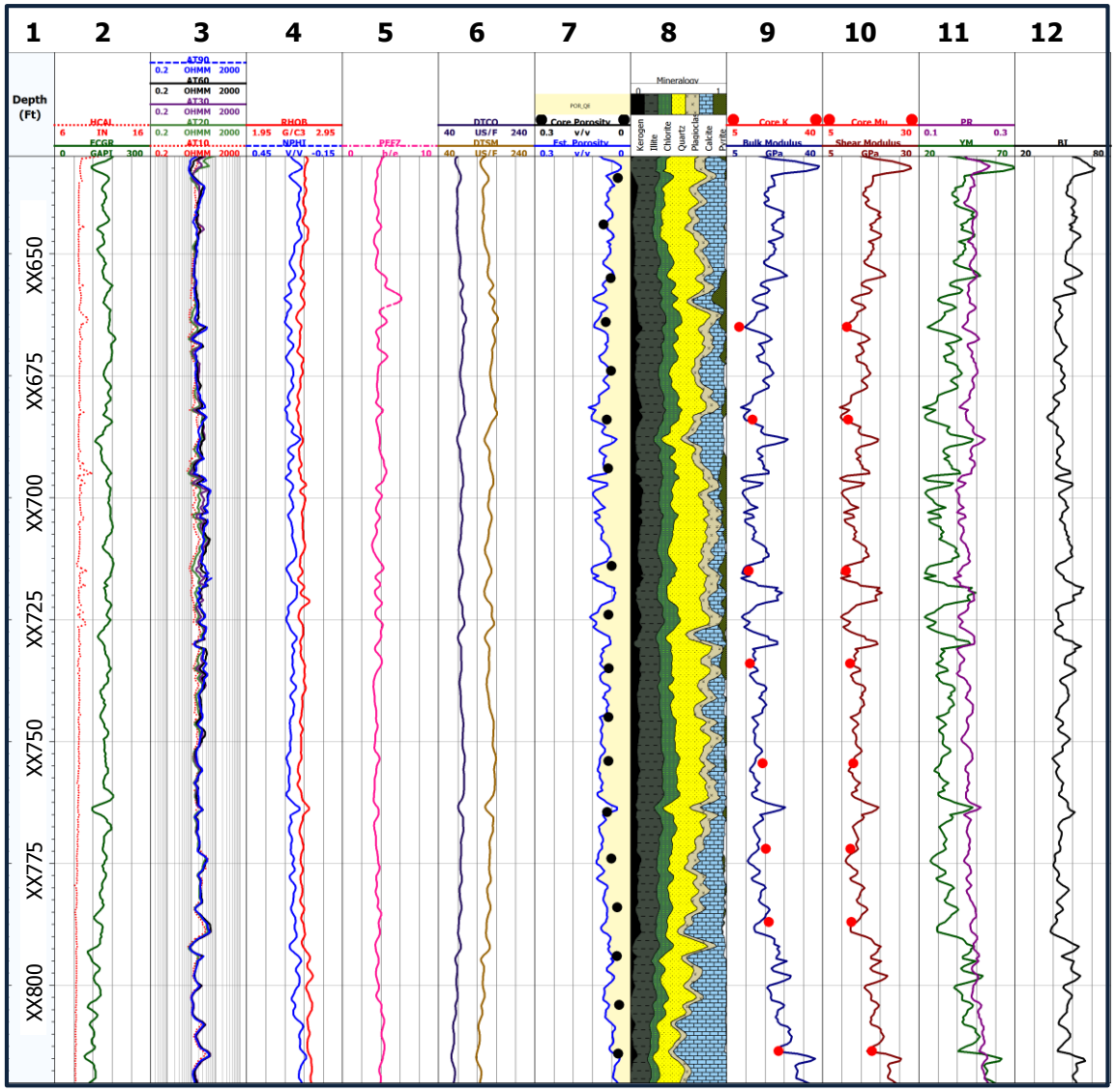

Figure 18: Conventional well logs and estimates of rock elastic properties in Well No 2. Tracks from left to right include, Track 1: Depth; Tracks 2-6: Caliper gamma ray, apparent resistivity, neutron porosity (in water-filled limestone porosity units), bulk density, PEF, and shear- and compressional-wave slowness; Track 7: well-log-based estimate of porosity, Track 8: Volumetric concentrations of minerals calculated using well logs; Tracks 9-11: Well-log-based estimate of bulk modulus, shear modulus, Young's Modulus and Poisson's Ratio. Track 12: Calculated brittleness index.

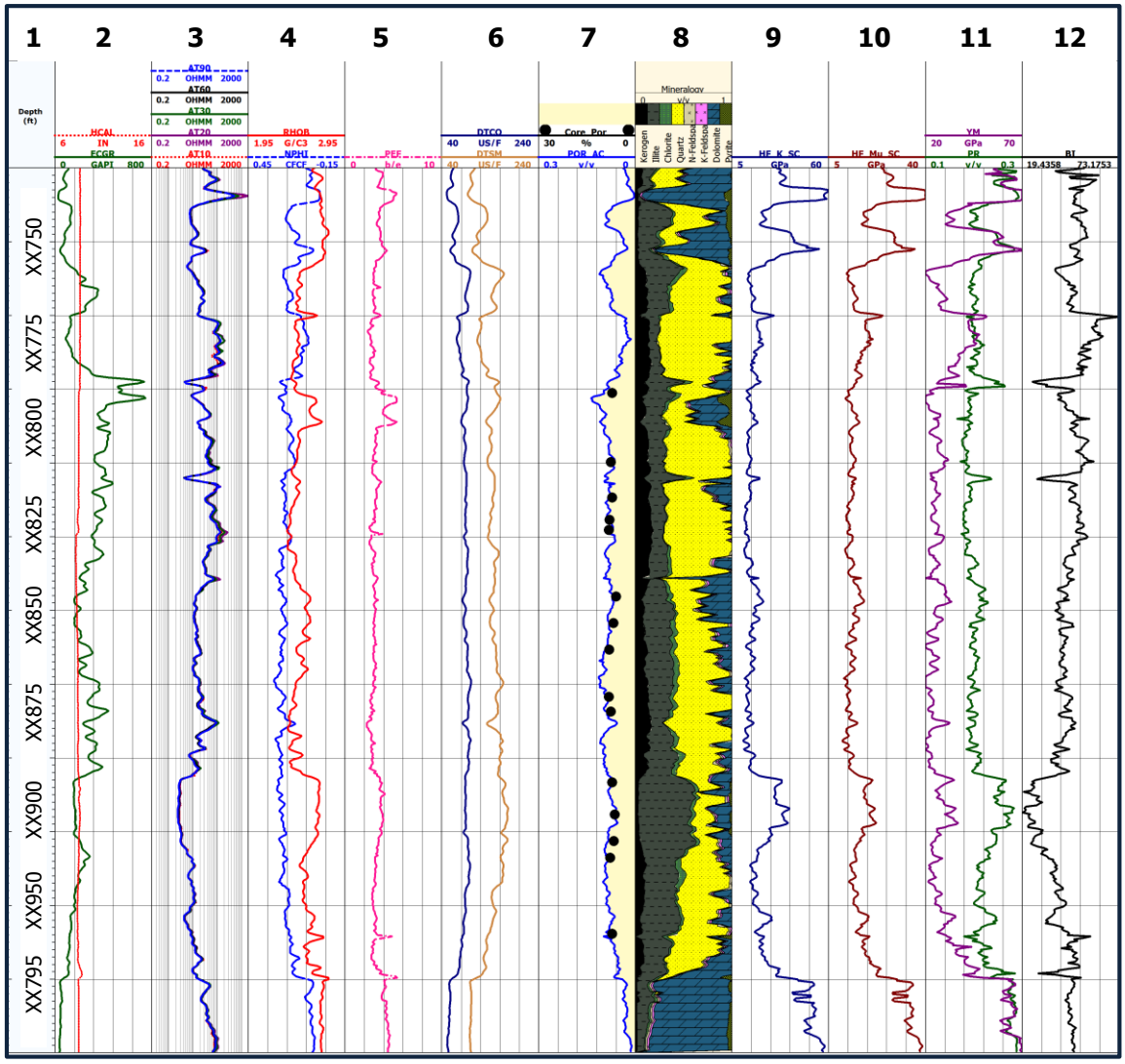

Figure 19: Conventional well logs and estimates of rock elastic properties in Well No. 3. Tracks from left to right include, Track 1: Depth; Tracks 2-6: Caliper gamma ray, apparent resistivity, neutron porosity (in water-filled limestone porosity units), bulk density, PEF, and shear- and compressional-wave slowness; Track 7: Well-log-based estimate of porosity, Track 8: Volumetric concentrations of minerals calculated using well logs; Tracks 9-11: Well-log-based estimate of bulk modulus, shear modulus, Young's Modulus and Poisson's Ratio. Track 12: Calculated brittleness index

5. ROCK CLASSIFICATION

This research accomplished an automatic rock classification by applying an unsupervised artificial neural network with inputs of (a) well logs including: resistivity, bulk density, neutron porosity, PEF, and compressional slowness and (b) well-log-based estimates: of volumetric concentration of quartz, illite, calcite, and dolomite, total porosity, brittleness index, and TOC concentration (wt.%).

Four rock classes were identified and used in the rock classification for wells in both the Haynesville shale (Well No.1 and Well No.2) and the Woodford shale (Well No. 3). For Well No.1 and Well No.2 the number of rock classes was determined based on the previous field studies (Hammes et al. 2011). For Well No. 3, this research based its approach on a study of the Woodford shale by Gupta et al. (2012) to determine the number of rock classes in this formation.

After applying an unsupervised artificial neural network to classify the roc, selecting which rock class should be identified as the most favorable rock for production can be challenging. A balance between advantageous mechanical properties, high TOC, and high porosity must be achieved. It would not be correct to select a brittle rock if the rock does not have any TOC concentration (wt.%), or the other way around. **Figures 20, 21,** and **22** show the identified rock classes for the wells evaluated in this research. Track 10 shows the rock classification results from well logs as inputs to the unsupervised neural network, and Track 11 shows the rock classification results of well-log-based calculated

properties of petrophysical, compositional, and elastic properties as inputs to the neural network.

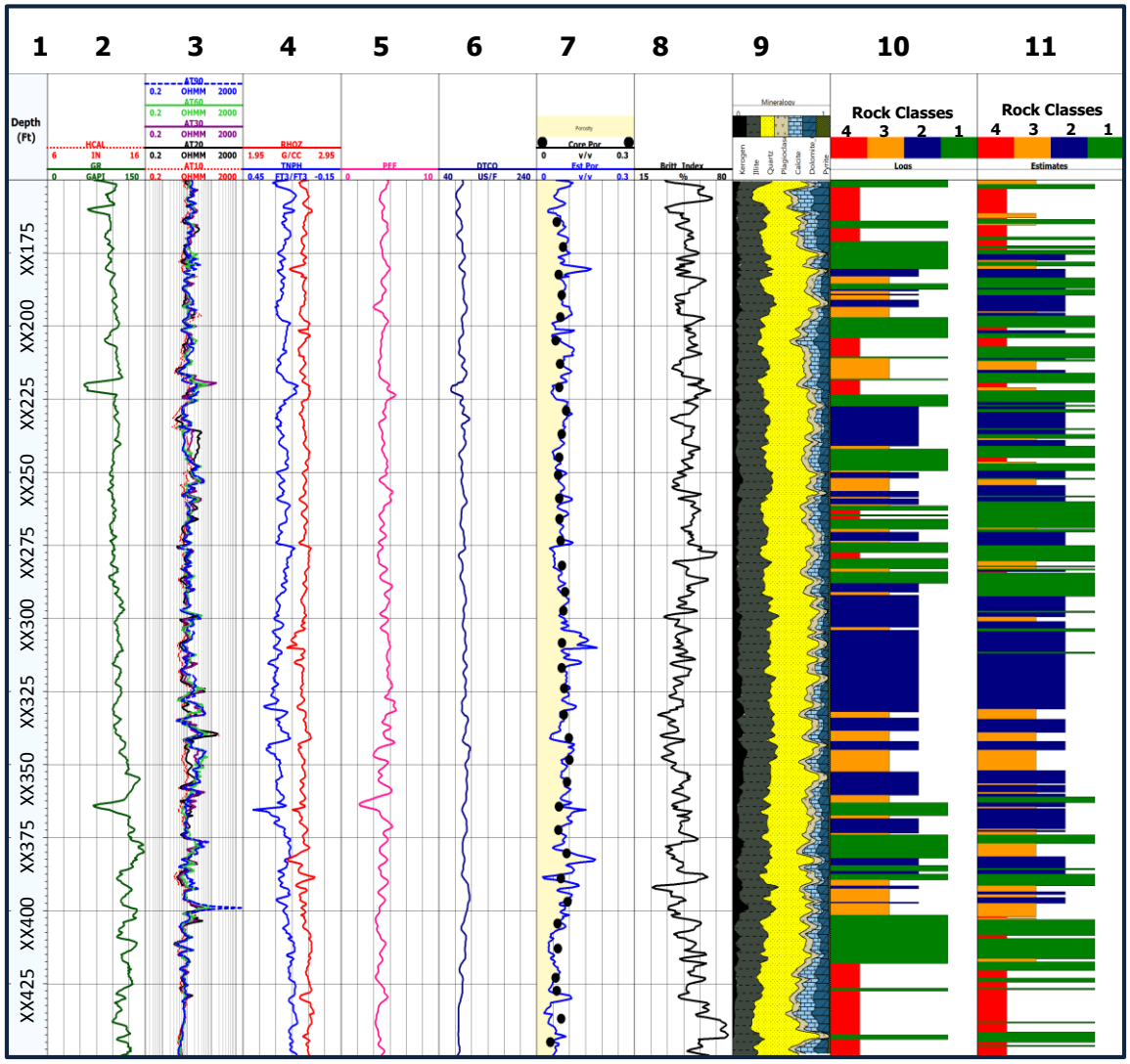

Figure 20: Rock classification in Well No. 1. Tracks from left to right include, Track 1: Depth; Tracks 2-6: Caliper gamma ray, apparent resistivity, neutron porosity (in water-filled limestone porosity units), bulk density, PEF, and shear- and compressional-wave slowness; Tracks 7: Well-log-based estimate of porosity, Track 8: Calculated brittleness index, Track 9: Volumetric concentrations of minerals calculated using well logs; Track 10: Rock classification using well logs as input; Track 11: Rock classification using calculated properties as input.

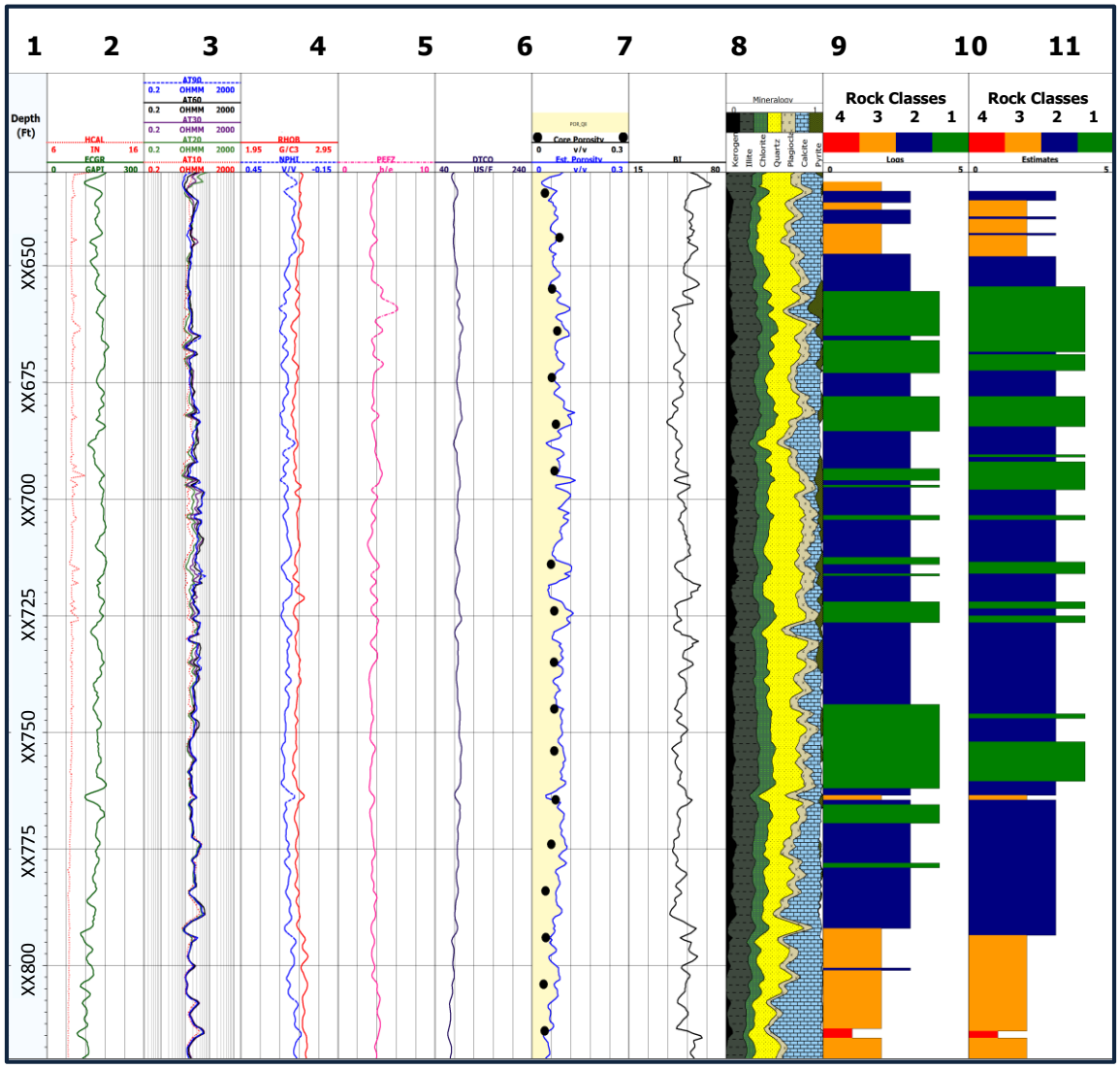

Figure 21: Rock classification in Well No. 2. Tracks from left to right include, Track 1: Depth; Tracks 2-6: Caliper gamma ray, apparent resistivity, neutron porosity (in water-filled limestone porosity units), bulk density, PEF, and shear- and compressional-wave slowness; Tracks 7: Well-log-based estimate of porosity, Track 8: Calculated brittleness index, Track 9: Volumetric concentrations of minerals calculated using well logs; Track 10: Rock classification using well logs as input; Track 11: Rock classification using calculated properties as input.

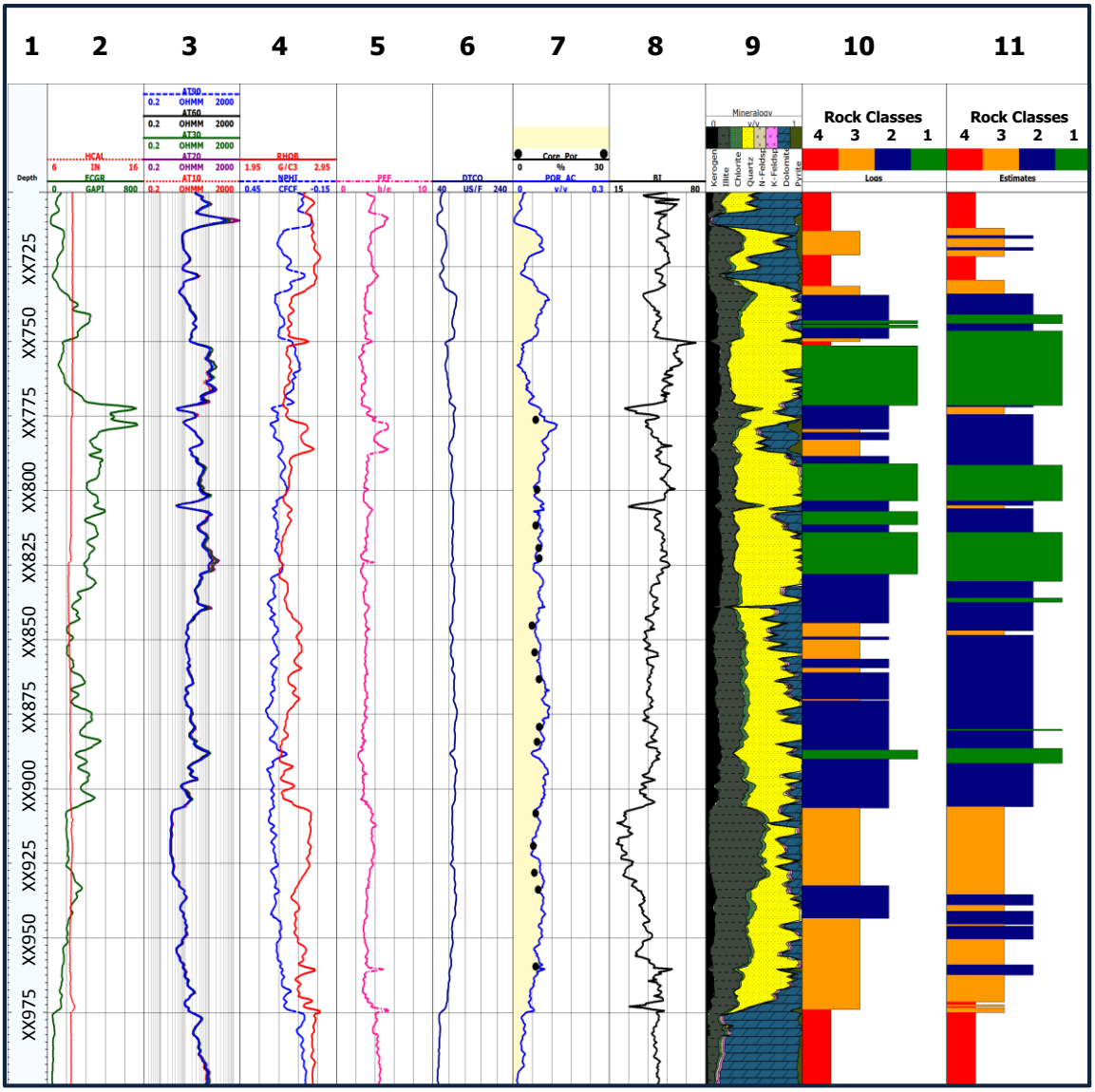

Figure 22: Rock classification in Well No. 3. Tracks from left to right include, Track 1: Depth; Tracks 2-6: Caliper gamma ray, apparent resistivity, neutron porosity (in water-filled limestone porosity units), bulk density, PEF, and shear- and compressional-wave slowness; Tracks 7: Well-log-based estimate of porosity, Track 8: Calculated brittleness index, Track 9: Volumetric concentrations of minerals calculated using well logs; Track 10: Rock classification using well logs as input; Track 11: Rock classification using calculated properties as input.

Figures 23, 24, and **25** show the distribution of the unitized properties of Rock Class 1, Rock Class 2, Rock Class 3, and Rock Class 4 in Well No. 1, Well No. 2, and Well No. 3, respectively. Rock Class 1 (green) was identified as the most favorable for hydraulic fracturing, on the hand Rock Class 4 (red) was identified as the least favorable rock for hydraulic fracturing.

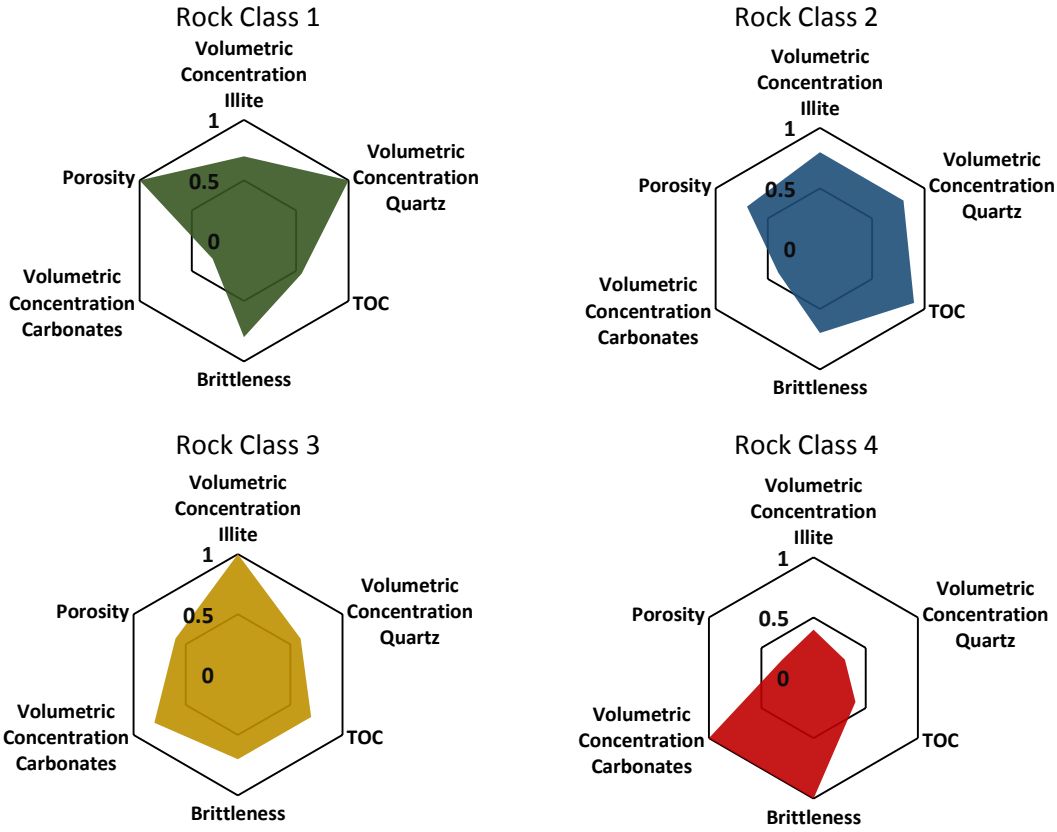

Figure 23: Distribution of the unitized rock properties in the identified Rock Classes in Well No. 1.

Rock Class 1 was selected as the most favorable rock because it contains high porosity, high volumetric concentration of quartz, and a high brittleness index compared to the other rock classes. On the other hand Rock Class 4 contains the lowest porosity out of the four rock classes and a high volumetric concentration of carbonates.

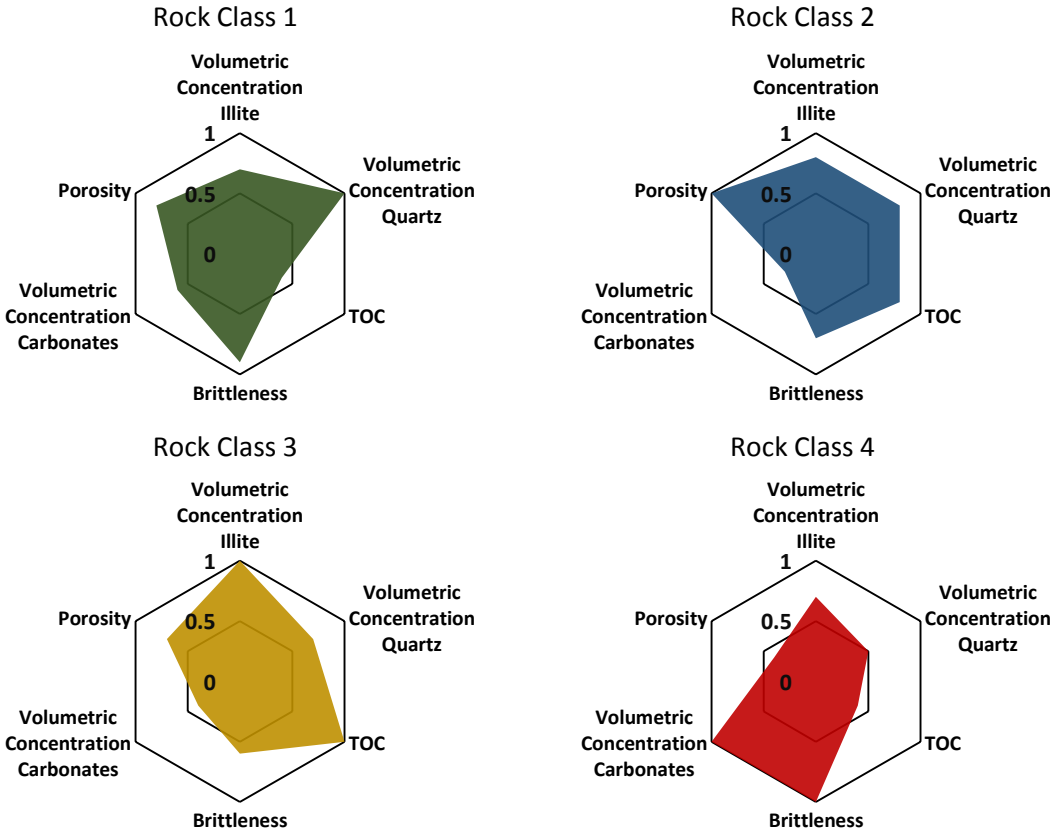

Figure 24: Distribution of the unitized rock properties in the identified Rock Classes in Well No. 2.

Rock Class 2 (blue) and Rock Class 3 (yellow) are the intermediate rock classes. Rock Class 2 was selected as more favorable for production than rock class 3 because it contains higher porosity and lower volumetric concentration of Illite compared to Rock Class 2.

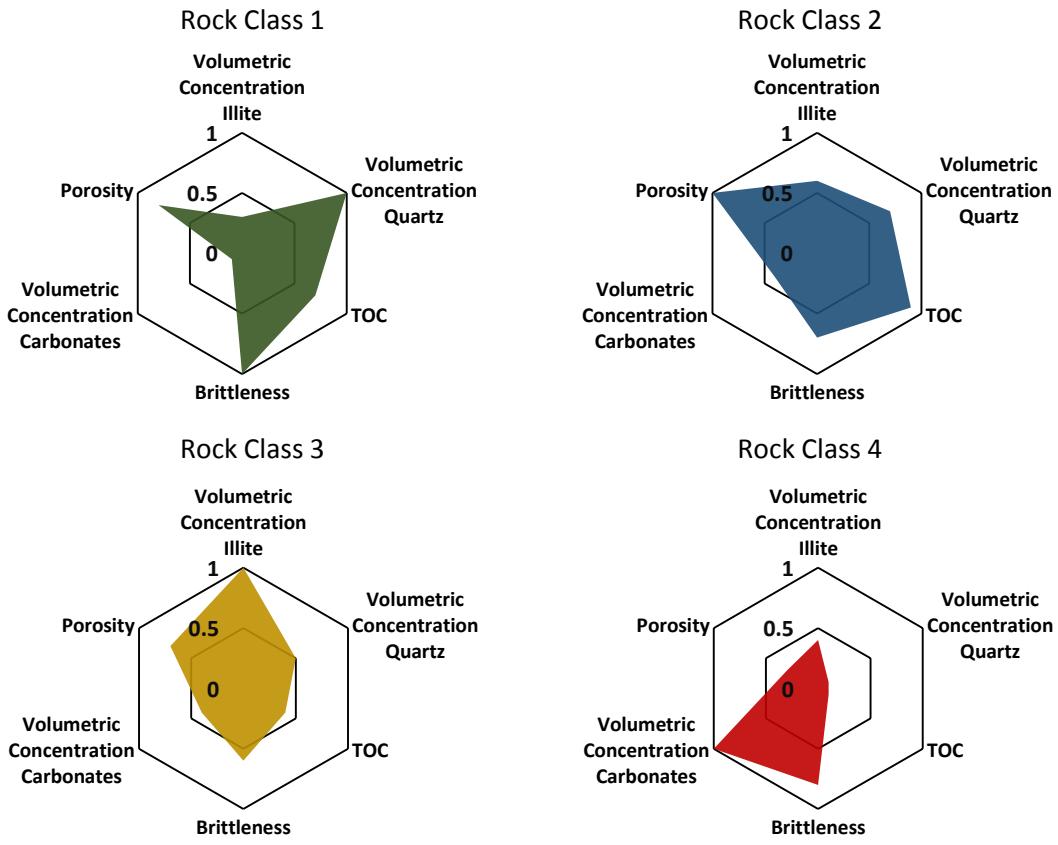

Figure 25: Distribution of the unitized rock properties in the identified Rock Classes in Well No. 3.

The results of rock classification using both well logs and well-log-based estimates of compositional, petrophysical, and elastic properties as input datasets remain almost

consistent, except in limited depth intervals. Not enough core measurements were available to prove the reliability of one of these approaches over the other one. However, having well logs as inputs to rock classification instead of calculated properties can provide more reliable rock classes, because of less uncertainty associated with the assumptions made for well-log interpretation and the estimation of elastic properties. The use of well logs can perform a faster classification that the use of calculated petrophysical, compositional, and elastic properties because neither the construction of a model nor calibration using core are required.

This research compared the identified rock classes in Well No. 1 and their corresponding thin-section images to lithofacies that were previously described in the Haynesville shale (Hammes and Frébourg 2012). Rock class 1 is the most organic-rich rock type and, therefore, corresponds to unlaminated peloidal siliceous facies.

An examination the thin-section images of this facies, revealed that the organic matter is randomly dispersed in the matrix among siliciclastic and carbonate grains. Furthermore, a comparison of the thin-section images showed that bioturbated siliceous facies is represented by Rock Class 2. The main characteristic of this facies is the apparent laminations of burrows and fine-grained siliceous grains, organics, carbonate, and clay. Rock Class 3 contains laminated peloidal siliceous facies, with a range of TOC between 2%-4% and a high brittleness index. The characteristics of this facies, observed from thin-section images, are organic laminae, sponge spicules, broken shells of bivalves, echinoderm fragments, peloids, and pellets (Hammes and Frébourg 2012). The organic-

poor facies corresponds to Rock Class 4, with the lowest TOC among all the facies. **Figure 26** shows thin-section examples of each of the classes.

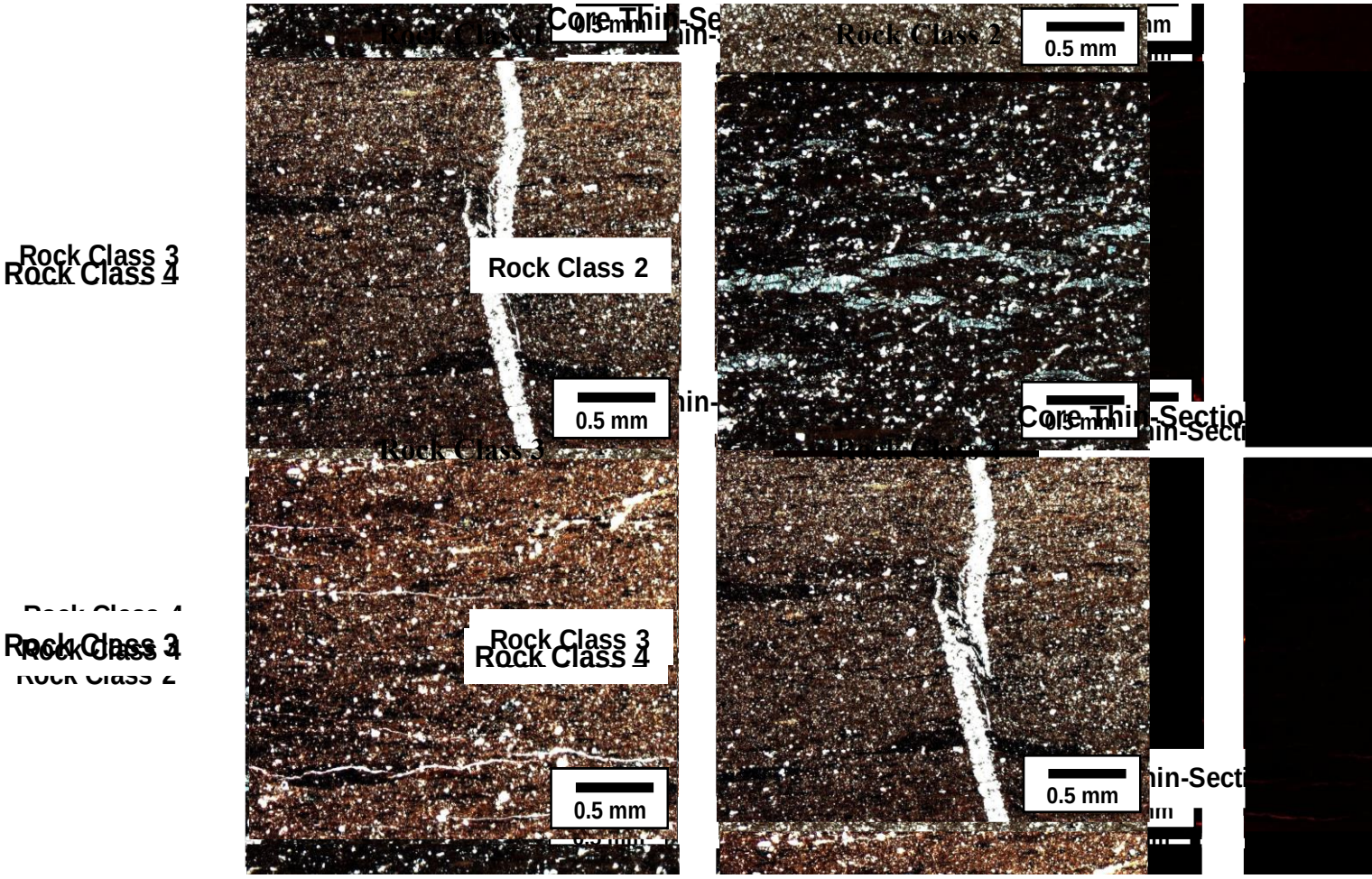

Figure 26: Comparison of the identified rock classes to core thin-section images at corresponding depth.

6. SUMMARY AND CONCLUSIONS

This section summarizes the main contributions of this work, provides the conclusions, and introduces recommendations for future work. The research outcomes fulfill the established objectives of this thesis.

6.1 Summary

The main objective of this thesis was to develop a well-log-based rock classification for organic shale reservoirs. First, this research jointly interpreted well logs and core measurements to develop a compositional and petrophysical model. This model was validated and calibrated using core measurements, and later applied to estimate the volumetric concentration of the minerals in the formation, the total porosity, and the water and hydrocarbon saturations using multi-mineral analysis.

Then, a study of distinct models to estimate the formation elastic properties was performed using seven different methods, which included (a) empirical correlations based on acoustic-wave velocity measurements, (b) Backus Average, (c) two approaches of the Self-Consistent Approximation (wet and dry), (d) two approaches of the Differential Effective Medium (wet and dry), and (e) DEM-SCA combined method. This research then compared the bulk and shear moduli of these models to tri-axial laboratory measurements. From this comparison, the Self-Consistent Approximation was proved to be the most

reliable model to estimate bulk and shear moduli in the two wells in the Haynesville shale, because it had the lowest relative error when compared to core measurements.

Using Young' Modulus and Poisson's Ratio, the brittleness index was calculated. The estimated depth-by-depth brittleness index is a depth-by-depth visual tool which is used to determine best candidate zones for hydraulic fracture treatment.

Finally, I used an unsupervised neural network to determine the rock classes the three wells studied. The inputs to the unsupervised neural network included (a) well-logs and (b) well-log-based estimates of compositional, petrophysical and elastic properties.

6.2 Conclusions

The petrophysical models built for the Haynesville shale and Woodford shales were calibrated and validated using core measurements. The estimates of TOC concentration (wt.%), water saturation, and total porosity showed errors of under 10% when compared to core measurements in all wells.

The estimates of volumetric concentrations of minerals, TOC concentration (wt.%), and total porosity were then used to estimate elastic properties of the formation using seven different approaches. Inclusion-based models showed up to 40% lower error than empirical equations and Backus Average when compared to shear modulus laboratory calculations. The Self-Consistent Approximation stood out as the most accurate inclusion-based model to estimate elastic properties in the formations studied; it showed errors of under 8.5% and 12.4% when estimating shear and bulk moduli, respectively.

Therefore, the Self-Consistent Approximation model can be used to properly estimate elastic properties in the studied organic-rich formations. The research completed for this thesis based the identified rock classes on formation-calculated compositional, petrophysical, and elastic properties. The incorporation of elastic properties in the rock classification helped identify the formation intervals capable of fracturing and maintaining a fracture. The rock class recognized as the most favorable for production in all wells studied contained total porosity of over 8%, brittleness over 48%, and the highest TOC concentration (wt.%) in the target intervals. The identified rock classes in Well No. 1 and their corresponding thin-section images, were compared to the identified lithofacies in the Haynesville shale (Hammes and Frébourg 2012) to validate the results.

An advantage of the introduced rock classification method over conventional core rock classification methods is its minimal dependency on core measurements, which makes it a faster tool for characterizing rock classes in organic-rich formations. Rock classification using both input datasets resulted in similar rock classes, leading to the conclusion that direct application of well logs can be effectively used for rock classification. Direct application of well logs reduces uncertainties associated with (a) the assumptions made for petrophysical and compositional evaluation on organic-rich formations and (b) the assumed rock physics models such as resistivity-porosity-saturation models and effective medium theories.

6.3 Recommendations for future work

The approach described in this thesis to estimate elastic properties is based on two fundamental assumptions. The first assumption considers that pore grains are treated as idealized ellipsoidal shapes. In reality, however, the shapes of the mineral grains are complex and non-uniform. Applying a variable grain aspect ratio could be used as an approach to take into account the inconsistency of the shapes when estimating bulk and shear moduli when using inclusion-based models. A comprehensive study on multiple high resolution Scanning Electron Microscope (SEM) images would provide a better understanding of individual shapes of the mineral inclusion minerals.

The second assumption considers that the formation is isotropic. Understanding the anisotropy of the Young's Moduli and Poisson's Ratios of shales is important for determining the change of *in-situ* stress of the formation. Apart from considering the mechanical or elastic properties in developing the petrophysical model, the formation stress profile plays an important role in the optimization of completion designs. The assumption of isotropy is commonly used for the estimation of *in-situ* stress because of challenges in anisotropic logging measurements. Development of dipole sonic measurements and stress models that account for anisotropy can improve the prediction of stress magnitudes. Taking into account stress models can further improve the identification optimal zones for economic fracture treatment & production design in organic-rich formations.

The rock classes in this thesis where categorized as favorable or not favorable based on petrophysical properties only. To have a more complete understanding of which rock class is the best one for hydraulic fracturing, it would be valuable to analyze the production data of each well studied. Comparing the rock classes with the depths where the lateral wells were landed and the hydrocarbon production of each of the wells will improve the best rock class selection.

REFERENCES

Amaefule, J.O., Altunbay, M., Tiab, D. Kersey, D.G., and Keelan, D.K. 1993. Enhanced Reservoir Description: Using Core and Log Data to Identify Hydraulic (Flow) Units and Predict Permeability in Uncored Intervals/Wells. Paper SPE 26436 presented at the SPE ATCE, Houston, Texas, USA, 3-6 October.

Ambrose, R., Hartman, R.C., Diaz-Campos M., Akkutlu, Y., and Sondergeld, C.H. 2010. New Pore-Scale Considerations for Shale Gas in Place Calculations. Paper SPE 131772 presented at the SPE Unconventional Gas Conference, Pittsburgh, Pennsylvania, USA, 23-25 February.

Avseth, P., Mukerji, T., Mavko, G., and Dvorkin, J. 2010. Rock-physics diagnostics of depositional texture, diagenetic alterations, and reservoir heterogeneity in high-porosity siliciclastic sediments and rocks - A review of selected models and suggested work flows. *Geophysics* **75** (1): A31–75A47

Backus, G. E. 1962. Long-wave Elastic Anisotropy Produced by Horizontal Layering: *Journal of Geophysical Research* **67** (11): 4427-4440.

Berryman, J.G. 1995. *Mixture Theories for Rock Properties*. 205-228. Washington, DC: American Geophysical Union.

Biot, M.A. 1956. Theory of Propagation of Elastic Waves in a Fluid-Saturated Porous Solid. 1. Low-Frequency Range. *The Journal of the Acoustic Society of America* **28** (2):168-178.

Birch, F. 1960. The Velocity of Compressional Waves in Rocks to 10 Kilobars. *Journal of Geophysical Research* **65** (4): 1083-1102.

Britt, L.K. and Schoeffler, J. 2009. The Geomechanics Of A Shale Play: What Makes A Shale Prospective. Paper prerented at the SPE Eastern Regional Meeting, Charleston, West Virginia, USA, 23-25 September.

Cardott, B.J. 2010. Application of Vitrinite Reflectance to Woodford Gas-Shale Plays in Oklahoma. Paper presentatet at the 2010 SIPES Annual Convention, Colorado Springs, Clorado, USA, 21-24 June.

Clavier, C., Coates, G., and Dumanoir, J. 1984. Theoretical and Experimental Bases for the Dual-Water Model for Interpretation of Shaly Sands. *Society of Petroleum Engineers Journal* **24** (2): 153-168.

Comer, R.D. 2008. Woodford Shale in Southern Midcontinent, USA - Transgressive System Tract Marine Source Rocks from Arid Passive Continental Margin with

Persistent Oceanic Upwelling. AAPG Search and Discover. Article 90078 presented at the Annual Convention, San Antionio, Texas, USA, 20-23 April.

Curtis, M.E., Ambrose, R.J., Sondergeld, C.H., and Rai, C.S. 2010. Structural Characterization of Gas Shales on the Micro- and Nano-Scales. Paper presented at the CSUG/SPE Conference, Calgary, Alberta, Canada, 19-21 October.

EIA. 2013. Technically Recoverable Shale Oil and Shale Gas Resources: An Assessment of 137 Shale Formations in 41 Countries Outside the United States. Report No. 20585, US DOI, Energy Information Administration, Washington, District of Columbia (13 June 2013).

Gamero-Diaz, H., Miller, C., and Lewis, R. 2013 sCore: A Mineralogy Bases Classification Scheme for Organic Mudstones. Paper SPE 166284 presented at the SPE ATCE, New Orleans, Louisiana, USA, 30 September - 2 October.

Gassmann, F. 1951. Graphical Evaluation of the Anomalies of Gravity and of the Magnetic Field, Caused by Three-dimensional Bodies. Paper presented at the 3rd World Petroleum Congress, The Hague, The Netherlands, 28 May-6 June.

Gupta, N., Rai, C.S., and Sondergeld, C.H. 2012. Integrated Petrophysical Characterization of the Woodford Shale in Oklahoma. Paper presented at the SPWLA 53rd Annual Logging Symposium, Cartagena, Colombia, 16-20 June.

Hammes, U. and Frébourg, G. 2012. Haynesville and Bossier Mudrocks: A Facies and Sequence Stratigraphic Investigation, East Texas and Louisiana. *Marine and Petroleum Geology* **31** (1): 8-26.

Hammes, U., Hamlin, H.S., and Ewing, T.E. 2011. Geologic Analysis of the Upper Jurassic Haynesville shalein East Texas and West Louisiana. *AAPG Bulletin* **95**: 1643-1666.

Heidari, Z., Torres-Verdin, C., and Pregg, W. E. 2012. Improved Estimation of Mineral and Fluid Volumetric Concentrations from Well Logs in Thinly Bedded and Invaded Formations. *Geophysics* **77** (3): 79-98.

Hornby, B.E., Schwartz, L.M., and Hudson, J.A. 1994. Anisotrpic Effective Medium Modeling of the Elastic Properties os Shales. *Geophysics* **59** (10): 1570-1583

Jarvie, D.M., Hill, R.J., Ruble, T.E.and Pollastro, R.M. 2007. Unconventional Shale-Gas Systems: The Mississippian Barnett Shale of North-Central Texas as One Model for Thermogenic Shale-Gas Assessment. *AAPG Bulletin* **91** (4): 475.

Jiang, M. and Spikes, K.T. 2013. Correlation between Rock Properties and Spatial Variations in Seismic Attributes for Unconventional Gas Shales – A Case Study on The Haynesville Shale. Paper presented at the SEG Annual Meeting, Houston Texas, USA, 22-27 September.

Jiang, M. and Spikes, K.T. 2011. Pore-Shape and Composition Effect on Rock-Physics Modeling in the Haynesville Shale. Paper presented at the 81st Annual SEG International Meeting. San Antonio, Texas, USA, 18-23 September

Kale, S., Rai, C.S., and Sondergeld, C.H. 2010. Rock Typing in Gas Shales. Paper SPE 134539 presented at the SPE ATCE, Florence, Italy, 19-22 September.

King, G. 2010. Thirty Years of Gas Shale Fracturing: What Have We Learned?. Paper SPE 133456 presented at the SPE ATCE, Florence, Italy, 19-22 September.

Kohonen, T. 1989. *Self-Organizinzation and Associative Memory,* 3rd edition. New York: Springer-Verlag.

Kvale, P.E. and Coffrey, B. 2010. Depositional Model for the Devonian Woodford Shale, SE Oklahoma, USA. AAPG Search and Discover. Aricle 90104 presented at the Annual Convention and Exhibition, 11-14 April.

Lee, S.H., Arun, K., and Datta-Gupta, A. 2002. Electrofacies Characterization and Permeability Predictions in Complex Reservoirs. *SPE Reservoir Evaluation & Engineering,* **5** (3): 237 - 248

Leverett, M.C. 1941. Capillary Behavior in Porous Solids. *Transactions of the AIME,* **142** (1): 159-172.

Marino, S., Herring, S., Stevens, K., Petriello, J., Handweger, D., Suarez-Rivera, R., and Woodruff, W. 2013. Paper SPE 167048 presented at the SPE Unconventional Conference and Exhibition Asia Pacific, Brisbane, Australia, 11-13 November.

Mavko, G., Mukerji, T. and Dvorkin, J. 2009. *The Rock Physics Handbook*, second edition.s Cambridge: Cambridge University Press.

Montaut, A., Sayar, P., and Torres-Verdin, C. 2013. Detection and Quatification of Rock Physics Properties for Improved Hydraulic Fracturing in Hydrocarbom-Bearing Shale. Paper presented at the SPWLA 54th Annual Logging Symposium, New Orleans, Luisiana, USA, 22-26 June.

Mullen, J., Lowry, J.C., and Nwabuoku K.C. 2010. Lessons Learned Developing the Eagle Ford Shale. Paper presented at the Tight Gas Completions Conference, San Antonio, Texas, USA, 2-3 November

Norris, A.1989. A Differential Scheme for the Effective Moduli of Composites. *Mechanics of Materials* **4** (1): 1-16.

Oh, K.T., Spikes, K. 2012. Velocity Modeling to Determine Pore Aspect Ratios of the Haynesville Shale. Paper SEG presented at the SEG Annual Meeting, Las Vegas Nevada, USA, 4-9 November.

Parker, M., Buller, D., Petre, E., and Dreher, D. 2009. Haynesville Shale-Petrophysical Evaluation. Paper SPE 122937 presented at the SPE Rocky Mountain Petroleum Technology Conference, Denver, Colorado, USA, 14-16 April.

Passey, Q. R., Creaney, S., Kulla, J.B., Moretti, F.J., and Stroud, J.D. 1990. A Practical Model for Organic Richness from Porosity and Resistivity Logs. *AAPG Bulletin*. **74** (12): 1777-1794.

Passey, Q.R., Bohacs, K.M., Esch, W.L., Klimentidis, R., and Sinha, S. 2010. From Oil-Prone Source Rock to Gas Producing Shale Reservoir—Geologic and Petrophysical Characterization of Unconventional Shale-Gas Reservoirs. Paper

SPE 131350 presented at the CPS/SPE International Oil & Gas Conference and Exhibition, Beijing, China, 8-10 June.

Pittman E.D. 1992. Relationship of Porosity and Permeability to Various Parameter Derived from Mercury Injection – Capillary Pressure Curves for Sandstones. *AAPG Bulletin* **76** (2): 191-198.s

Popielski, A.C., Heidari, Z., and Torres-Verdin, C. 2012. Rock Classification from Conventional Well Logs in Hydrocarbon-Bearing Shale. Paper SPE 159255 presented at the SPE ATCE, San Antonio, Texas, USA, 8-10 October.

Potma, K., Jonk, R., Advie, N., and Austin, N. 2013. Integrated Geological, Petrophysical, and Geophysical Characterization of a World Class Shale Gas Play, Horn River Basin, British Columbia, Canada. Paper IPTC 16784 presented at the International Petroleum Technology Conference, Beijing, China, 26-28 March.

Quirein, J., Witkowsky, J., Truax, J., Galford, J., Spain, S., and Odumosu, T. 2010. Integrating Core Data and Wireline Geochemical Data for Formation Evaluation and Characterization of Shale Gas Reservoirs. Paper SPE 134559 presented at the SPE ATCE, Florence, Italy, 19-22 September.

Ramirez, T.R., Klein, J.D., Bonnie, R.J.M., and Howard, J.J., 2011, Comparative

Study of Formation Evaluation Methods for Unconventional Shale-Gas Reservoirs: Application to the Haynesville shale(Texas): Paper SPE 144062, Proceedings of the SPE North American Unconventional Gas Conference and Exhibition, The Woodlands, Texas, USA, 14-16 June.

Rickman, R., Mullen, M., Petre, E., Grieser, B., and Kundert, D. 2008. A Practical Use of Shale Petrophysics for Stimulation Design Optimization: All Shale Plays Are Not Clones of the Barnett Shale. Paper SPE 115258 presented at the SPE ATCE, Denver, Colorado, USA, 21-24 September.

Saggaf M.M. and Marhoon M.I. 2001. Seismic Facies Mapping by Competitive Neural Networks. Paper presented at the SEG Internationsl Exposition and Annual Meeting San Antonio, Texas, USA, 9-14 September.

Skalinski, M., Gottlib-Zhe, S., and Moss., B. 2005. Defining and Predicting Rock Types in Carbonates-an Integrated Approach using Core and Log Data in Tengiz Field. Paper presented at the SPWLA 46th Annual Logging Symposium, New Orleans, Louisiana, USA, 26-29 June.

Sondergeld, C.H., Ambrose, R.J., Rai, C.S., and Moncrief, J. 2010. Micro-Structural Studies of Gas Shales. Paper SPE 131771 presented at the SPE Unconventional Gas Conference, Pittsburgh, Pennsylvania, USA, 23-25 February.

Silva, F.P., Ghano, A.A., and Al Mansoori, A. 2002 Rock Type Constrained 3D Reservoir Characterization and modeling Paper SPE 78504 presented at the International Petroleum Exibition and Conference, Abu Dhabi, UAE, 13-16 November

Singh, S., Qiu, F., Morgan, N., Nath, T., and Pritchard, T. 2013. Critical Comparative Assessment of a Novel Approach for Multi-Mineral Modeling in Shale Gas: Results from an Evaluation Study in Marcellus Shale. Paper SPE 167037 presented at the SPE Unconventional Resources Conference and Exhibition, Brisbane, Australia, 11-13 November.

Ye, S.J., Rabiller, P., and Keskes. 1998. Automatic High Resolution Texture Analysis on Borehole Imagery. Paper presented at the SPWLA 39th Annual Logging Symposium, Denver Colorado, USA, 26-28 May

Zimmerman, R.W. 1991. Elastic Moduli of a Solid Containing Spherical Inclusions. *Mechanics of Materials* **12** (1): 17–24.